nature chemical biology

ARTICLES

https://doi.org/10.1038/s41589-020-0557-2

Manumycin polyketides act as molecular glues between UBR7 and P53

Yosuke Isobe[1,2], Mikiko Okumura[1,2], Lynn M. McGregor[3], Scott M. Brittain[3], Michael D. Jones[3], Xiaoyou Liang[3], Ross White[1,2], William Forrester[3], Jeffrey M. McKenna[2,3], John A. Tallarico[2,3], Markus Schirle[2,3], Thomas J. Maimone[1,2] ✉ and Daniel K. Nomura[1,2,4,5,6] ✉

Molecular glues are an intriguing therapeutic modality that harness small molecules to induce interactions between proteins that typically do not interact. However, such molecules are rare and have been discovered fortuitously, thus limiting their potential as a general strategy for therapeutic intervention. We postulated that natural products bearing one or more electrophilic sites may be an unexplored source of new molecular glues, potentially acting through multicovalent attachment. Using chemoproteomic platforms, we show that members of the manumycin family of polyketides, which bear multiple potentially reactive sites, target C374 of the putative E3 ligase UBR7 in breast cancer cells, and engage in molecular glue interactions with the neosubstrate tumor-suppressor TP53, leading to p53 transcriptional activation and cell death. Our results reveal an anticancer mechanism of this natural product family, and highlight the potential for combining chemoproteomics and multicovalent natural products for the discovery of new molecular glues.

The challenge of tackling the undruggable proteome has inspired the development of innovative technologies that enable functional targeting of biomolecules with new therapeutic modalities. Examples of some of these small-molecule-based technologies include chemoproteomics-enabled covalent ligand screening and DNA-encoded libraries for discovering ligands against undruggable proteins, proteolysis-targeting chimeras (PROTACs) or degraders for targeted ubiquitin–proteasome system-dependent degradation of proteins, and 'molecular glues' for small-molecule-induced formation of protein interfaces that confer enhanced, inhibited or new protein function[1–6]. Molecular glue-based degraders, as exemplified by the IMiD family of immunomodulatory drugs, including thalidomide, are notable for their potentially lower molecular mass compared with linker-based bifunctional molecules (for example, PROTACs), a possible advantage for increased bioavailability and improved pharmacokinetic profiles[4]. Moreover, molecular glues are also particularly interesting from a functional perspective, because the few well-characterized examples uniquely modulate protein function and downstream biology by stabilizing protein complexes between binding partners that would not otherwise interact.

Three notable molecular glues showcase diverse functional outcomes associated with new protein complexes. The natural product rapamycin binds to FKBP12, leading to the recruitment of the mammalian target of rapamycin complex 1 (mTORC1), resulting in its partial inhibition[7]. The cotylenin diterpenes form interfaces between the 14-3-3 protein family and a variety of interacting partners[8]. Thalidomide binds to the E3 ligase cereblon to form a new protein interface that recruits neosubstrates such as SALL4 or Ikaros transcription factors for ubiquitination and degradation[9–12]. Paradoxically, degradation of the former leads to teratogenic effects whereas degradation of the latter is a proven chemotherapeutic strategy[4,6]. Moreover, analogs of rapamycin and thalidomide can still maintain binding to FKBP12 and cereblon, respectively, but shift their neosubstrate-binding profiles to confer new and distinct biological functions[13,14]. This realization has led to the discovery of approved drugs such as lenalidomide, pomalidomide and FK506. Unfortunately, only a handful of well-characterized molecular glues has been discovered, thus limiting our understanding of the design principles behind their function and reducing their impact on drug discovery. Natural products have been a robust source of many known molecular glue interactions (for example, rapamycin, FK506, auxin, brefeldin A and forskolin), and their diverse and stereochemically rich architectures possess many positive attributes for recruiting protein surfaces[5,6].

Electrophilic natural products represent a vastly underexplored subset of natural products from which molecular glues can originate, and such species could have unique and positive attributes owing to their potential for covalent bond formation[15]. Although covalently acting natural products have not been previously identified as molecular glues, we hypothesized that natural products, which (1) bear one or more potential sites for covalent interaction with nucleophilic amino acids on proteins and (2) have also been shown to possess biological activity, would constitute candidates for possessing potentially unique, glue-like characteristics.

The covalence of these potential natural-product-based molecular glues also enables rapid mechanistic deconvolution of protein targets using chemoproteomic platforms. One such platform used in the present study is activity-based protein profiling (ABPP), which uses reactivity-based chemical probes to profile proteome-wide reactive, functional and ligandable hotspots directly in complex living systems. When used in a competitive manner, covalently acting small molecules can be competed against the binding of reactivity-based probes, to facilitate the identification of their protein targets and covalent sites of modification[1,2,16]. On identifying

[1]Department of Chemistry, University of California, Berkeley, Berkeley, CA, USA. [2]Novartis-Berkeley Center for Proteomics and Chemistry Technologies, Berkeley, CA, USA. [3]Novartis Institutes for BioMedical Research, Cambridge, MA, USA. [4]Department of Molecular and Cell Biology, University of California, Berkeley, Berkeley, CA, USA. [5]Department of Nutritional Sciences and Toxicology, University of California, Berkeley, Berkeley, CA, USA. [6]Innovative Genomics Institute, Berkeley, CA, USA. ✉e-mail: maimone@berkeley.edu; dnomura@berkeley.edu

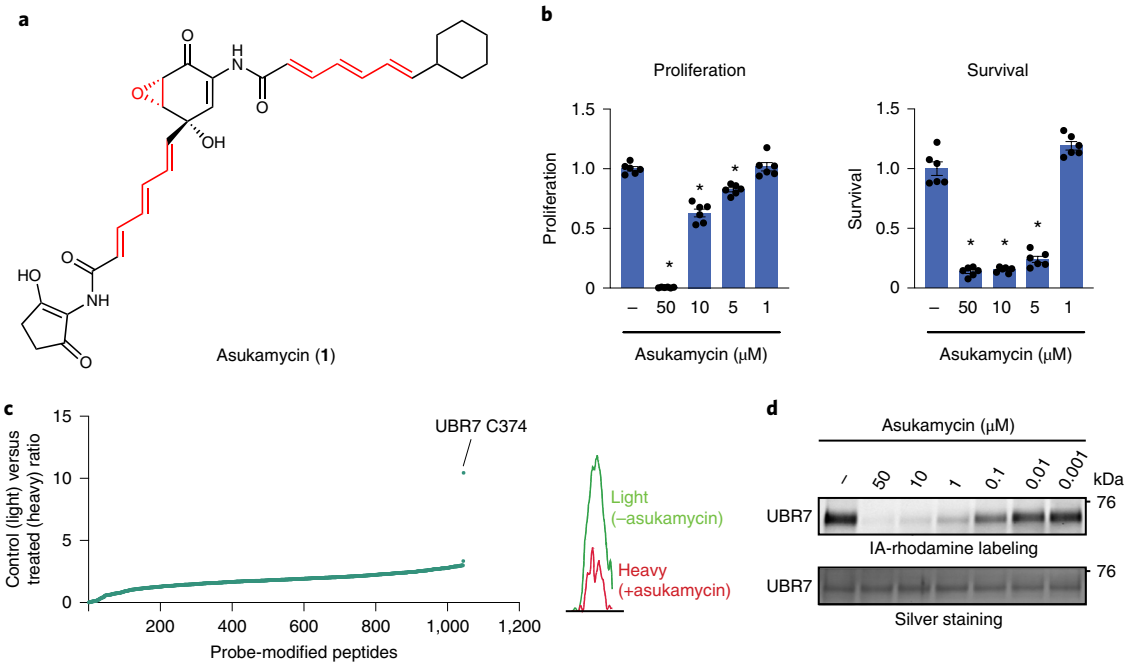

Fig. 1 | Asukamycin targets C374 of UBR7 in breast cancer cells. a, Structure of asukamycin highlighting (in red) three potentially reactive sites. **b**, Proliferation and serum-free cell survival in 231MFP breast cancer cells treated with DMSO vehicle or asukamycin for 48 h, assessed using the Hoechst stain. **c**, IsoTOP-ABPP analysis of asukamycin in situ in 231MFP cells. Such cells were treated with DMSO vehicle or asukamycin (10 μM) for 3 h, and the resulting cell lysates were labeled with IA-alkyne (100 μM) for 1 h, after which point isotopically light (control) or heavy (asukamycin-treated) TEV, tag-bearing, biotin–azide handles were appended by CuAAC and taken through the isoTOP-ABPP method. The light:heavy ratios of probe-modified peptides are shown, as well as the average probe-modified peptide ratios. On the right is a representative MS1 chromatogram of the probe-modified, C374-bearing, UBR7 peptide between control versus asukamycin-treated cells. These data represent data from $n = 3$ biologically independent samples. **d**, Gel-based ABPP analysis of asukamycin against pure human UBR7 protein. UBR7 protein was preincubated with DMSO vehicle or asukamycin for 30 min before IA-rhodamine (200 nM) labeling of UBR7 for 1 h at room temperature. Protein was resolved by SDS–PAGE and visualized by in-gel fluorescence, and protein loading was assessed by silver staining. Data shown in **b** are individual replicate values and mean ± s.e.m. ($n = 6$ biologically independent samples per group). Gels shown in **d** are representative of blots from $n = 3$ biologically independent samples per group. Statistical significance was calculated using two-tailed, unpaired Student's *t*-tests and shown as $^*P < 0.05$ compared with vehicle-treated controls within each group. Source data for cropped blots and bar graphs are provided.

the direct targets of the natural product, standard pulldown and quantitative proteomic profiling experiments can be used to identify specific molecular glue interactions enabled by the natural product.

In the present study, we interrogated the *Streptomyces*-derived family of manumycin polyketide natural products, specifically asukamycin (**1**) and manumycin A (**2**), which have documented antibiotic and antiproliferative properties[17]. Manumycin A has also been shown to inhibit farnesyl transferase activity and sphingomyelinase activity, but asukamycin is not known to inhibit these targets and its anticancer mechanism of action is unclear[18–22]. These molecules possess a suite of electrophilic sites that could potentially react covalently with nucleophilic amino acids within proteins, such as cysteines (Fig. 1a)[18]. We hypothesized that multiple reactive sites within these natural products may lead to specific interactions with multiple protein targets, resulting in bifunctional or molecular glue-type interactions.

Using ABPP-based chemoproteomic platforms, we demonstrate that one of the primary targets of asukamycin is C374 of the postulated E3 ubiquitin ligase UBR7. We further showed that this UBR7–asukamycin complex engages multiple proteins in breast cancer cells, including the tumor-suppressor TP53, and that the resulting UBR7–asukamycin–TP53 complex contributes to the anticancer activity of asukamycin.

Results

Anticancer activity of asukamycin. There is an unmet medical need for new triple-negative breast cancer (TNBC) therapies because such malignancies have worse clinical prognoses than other breast cancer subtypes. Moreover, few targeted therapies are approved for the treatment of TNBCs. New small molecules, mechanisms and therapeutic modalities for combatting TNBCs could greatly reduce the mortality associated with these aggressive breast cancers[23]. We show that asukamycin impairs the proliferation (with full serum-containing medium) and serum-free cell survival of two TNBC-derived cell lines, 231MFP and HCC38 (Fig. 1b and see Supplementary Fig. 1), with 50% effective concentration (EC_{50}) values of 13.8 and 4.5 μM for 231MFP proliferation and survival, respectively. The apparent difference in sensitivity observed with asukamycin antiproliferative and antisurvival effects in 231MFP cells were probably due to asukamycin binding to serum in the medium, because the relative levels of intracellular asukamycin were much higher in 231MFP cells in serum-free medium, compared with serum-containing medium (see Supplementary Fig. 1). The apparent low cell-based potency may also be due to low free asukamycin exposure in cells because of its high lipophilicity, as well as low cellular permeability, due to its higher molecular mass and high number of rotatable bonds. We also tested asukamycin growth inhibitory effects across 250 cancer cell lines, spanning many different tumor types, and showed broad growth inhibitory effects across many cancer cell lines with concentrations values at which a 50% growth inhibition was observed (GI_{50}) of from 0.08 μM to >30 μM (see Extended Data Fig. 1a). Among the 19 breast cancer cell lines tested from receptor-positive and TNBC cell lines, 7 showed heightened sensitivity with GI_{50} values of 5.7–11.2 μM, 9 showed

intermediate sensitivity with GI_{50} values of 13–16 μM and 3 showed refractory effects with GI_{50} values >20 μM, in which HCC38 and the MDA-MB-231 line, from which 231MFP cells were derived, showed intermediate sensitivity (see Extended Data Fig. 1b,c). Given our interest in TNBCs, we focused our subsequent mechanistic studies for asukamycin on 231MFP cells, as a representative TNBC cell line.

ABPP to map asukamycin targets. We postulated that the antiproliferative activity of asukamycin may depend on covalent interactions with cysteines on specific protein targets. Asukamycin could react with protein nucleophiles through either hetero-Michael addition reactions with one or both of the two poly(unsaturated amide) side chains or reaction with the epoxyketone moiety, a known process for similar epoxyketone natural products[24]. We performed ABPP-based chemoproteomic profiling to identify asukamycin targets in 231MFP TNBC cells. Proteome samples treated with vehicle or asukamycin were labeled with the cysteine-reactive probe iodoacetamide alkyne (IA-alkyne or *N*-hex-5-ynyl-2-iodoacetamide), before further processing using a well-validated method for covalent ligand target identification—isotopic tandem orthogonal proteolysis ABPP (isoTOP-ABPP)[2,16,25]. We identified C374 of UBR7 as a primary target of asukamycin with the highest control:treated (or light:heavy) ratio in 231MFP cells (Fig. 1c). We confirmed that UBR7 was a direct target of asukamycin using gel-based ABPP approaches, wherein we show competition of asukamycin against rhodamine-functionalized iodoacetamide (IA-rhodamine) labeling of recombinant human UBR7 protein (Fig. 1d).

Next, we investigated whether the anticancer effects of asukamycin were driven through asukamycin interactions with C374 of UBR7. Stable UBR7 knockdown in 231MFP cells did not compromise proliferation, but conferred complete resistance to asukamycin-mediated antiproliferative effects (Fig. 2a,b). Expression of wild-type (WT) or C374A mutant UBR7 in small hairpin (sh)UBR7 231MFP cells led to re-sensitization of asukamycin-mediated, antiproliferative effects in WT, but not C374A, UBR7-expressing cells (Fig. 2c). Taken together, these results demonstrate that asukamycin targets C374 of UBR7 and that this interaction is responsible for the antiproliferative effects of asukamycin in breast cancer cells. These data also hinted that asukamycin, through targeting C374 of UBR7, may be conferring a gain-of-function effect, because UBR7 knockdown itself does not impair cell proliferation (see Supplementary Fig. 2). Further supporting this hypothesis, we found that overexpression of WT, but not C374A mutant, FLAG–UBR7 conferred significantly heightened, asukamycin-induced antiproliferative effects with EC_{50} values of 10.0, 4.7 and 10.0 μM for green fluorescent protein (GFP), WT UBR7 and C374A mutant, UBR7-expressing 231MFP cells, respectively (Fig. 2d,e).

Although UBR7 is annotated as an E3 ubiquitin ligase and postulated to be involved in histone ubiquitination[26], its biochemical and physiological functions are poorly understood, especially with regard to cancer cell proliferation. We attempted to reconstitute the activity of UBR7 in vitro, but our various efforts to demonstrate UBR7 activity failed. Instead, we next explored the potential for UBR7 to engage in asukamycin-induced interactions with other proteins.

Mapping molecular glue interactions of UBR7–asukamycin. From these results and the potential for asukamycin to achieve multiple covalent interactions, we postulated that asukamycin may be conferring gain-of-function effects on UBR7 through engaging in molecular glue interactions with other proteins. To substantiate this hypothesis, we performed proteomic analysis on anti-FLAG pulldown eluate from FLAG–GFP- or FLAG–UBR7-expressing 231MFP cells, treated with vehicle or asukamycin to identify protein–protein interactions that were dependent on both UBR7 and asukamycin. From this experiment, we identified 13 proteins that showed significant ($P<0.01$) and >15-fold higher pulldown in the asukamycin-treated FLAG–UBR7 cells compared with vehicle-treated FLAG–UBR7 cells (Fig. 3a). Among these 13 targets, 8 are UBR7 dependent, with more than a four-fold enrichment between asukamycin-treated FLAG–UBR7 cells and asukamycin-treated FLAG–GFP cells (Fig. 3a). These eight targets include proteins of great importance in cancer, including DNA protein kinase (PRKDC) and the tumor-suppressor p53 (TP53)[27,28] (Fig. 3b). In pulldown experiments, we confirmed the asukamycin-dependent interactions with UBR7 using western blots that showed that proteins such as TP53 and PRKDC interacted specifically in FLAG–UBR7-expressing cells treated with asukamycin (Fig. 3c).

It is interesting that, in our anti-FLAG blot from FLAG–UBR7 pulldown studies, we also observed several higher-molecular-mass species in a reducing sodium dodecylsulfate–polyacrylamide gel electrophoresis (SDS–PAGE) gel that corresponded to the estimated combined masses of FLAG–UBR7 and TP53, as well as even higher-molecular-mass species that corresponded to the estimated molecular mass of PRKDC (Fig. 3c). In the anti-TP53 blot from the same pulldown studies, in addition to the expected TP53 band, we also observed a distinct higher-molecular-mass species that corresponded to a molecular mass in line with the addition of FLAG–UBR7 and TP53 (Fig. 3c). Reinforcing that this higher-molecular-mass FLAG–UBR7 band included the TP53 higher-molecular-mass species, a dual-color western blot showed overlap between the FLAG–UBR7 and TP53 higher-molecular-mass bands (see Supplementary Fig. 3). Proteomic analysis of this higher-molecular-mass region further confirmed significantly increased levels of TP53 and UBR7 in this 100- to 140-kDa range (see Extended Data Fig. 2). UBR7 knockdown in 231MFP cells treated with asukamycin also resulted in >80% reduction in the higher-molecular-mass TP53 species compared with shControl counterparts (Fig. 3d, and see Extended Data Fig. 3a). TP53 knockdown in 231MFP cells treated with asukamycin resulted in a significant, albeit less pronounced, reduction in the higher-molecular-mass FLAG–UBR7 species compared with shControl counterparts (see Extended Data Fig. 3b,c). Although there may be additional proteins of similar molecular mass to TP53 that are included in this higher-molecular-mass FLAG–UBR7 species, we believe that TP53 is one of these proteins. Further confirming that this higher-molecular-mass TP53 species is a ternary complex of UBR7, asukamycin and TP53, interactions with the higher-molecular-mass TP53 complex was completely lost and interactions with the parent molecular-mass TP53 were significantly reduced from pulldown of C374A mutant FLAG–UBR7 compared with WT FLAG–UBR7 in 231MFP cells (see Extended Data Fig. 4). The higher-molecular-mas TP53 species in the input for both WT and C374A mutant FLAG–UBR7 lines is probably the ternary complex arising from endogenous WT UBR7 in the FLAG–UBR7 C374A mutant-expressing cells.

We further confirmed that these higher-molecular-mass species were not polyubiquitinated TP53 because treatment of proteomes with the deubiquitinase USP2 could not eliminate these higher-molecular-mass TP53 bands (see Supplementary Fig. 4). These results show enrichment of both the parent molecular-mass protein interaction partner and a higher-molecular-mass species, suggesting that the complexes between UBR7–asukamycin and binding partners such as TP53 or PRKDC initially form through reversible interactions, which eventually in part lead to multicovalent interactions. We also showed that abundant proteins such as glyceraldehyde 3-phosphate dehydrogenase (GAPDH) did not interact with the asukamycin–UBR7 complex, arguing for specific molecular interactions over nonspecific-binding events (Fig. 3c). Although TP53 was not identified as a target in our isoTOP-ABPP studies, probably due to its low abundance, we further demonstrated that asukamycin directly interacts with TP53 using gel-based ABPP (Fig. 3e).

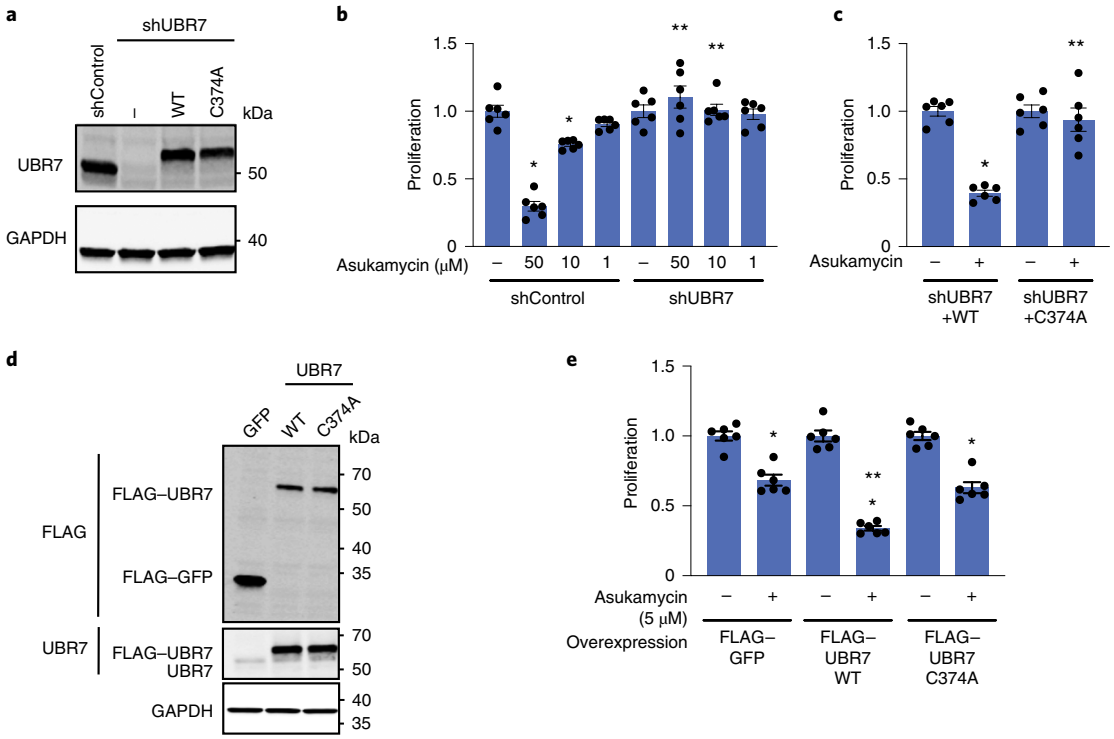

Fig. 2 | Asukamycin impairs breast cancer cell proliferation through targeting UBR7. a, Expression of UBR7 and loading control GAPDH levels in 231MFP shControl, shUBR7 or shUBR7 cells expressing FLAG-tagged WT or FLAG-tagged C374A mutant UBR7 protein, assessed using western blotting. **b**, Cell proliferation in 231MFP shControl or shUBR7 cells treated with DMSO vehicle or asukamycin for 24 h, assessed using the Hoechst stain. **c**, Cell proliferation in 231MFP shUBR7 cells expressing FLAG-WT or FLAG-C374A mutant UBR7 treated with DMSO vehicle or asukamycin (50 μM) for 24 h. **d**, Anti-FLAG, anti-UBR7 and loading control anti-GAPDH protein expression in 231MFP cells stably expressing FLAG-GFP, FLAG-UBR7 WT or FLAG-UBR7 C374A mutant assessed using western blotting. **e**, Cell proliferation of 231MFP cells transiently expressing FLAG-GFP, FLAG-UBR7 WT or a FLAG-UBR7 C374A mutant treated with DMSO or asukamycin (5 μM) for 48 h, assessed using the Hoechst stain. Data shown in **b**, **c** and **e** are individual replicate values and mean ± s.e.m. ($n = 6$ biologically independent samples per group). Gels shown in **a** and **d** are representative blots from $n = 3$ biologically independent samples per group. Statistical significance was calculated using two-tailed, unpaired Student's *t*-tests and shown as: $^{*}P < 0.05$ compared with vehicle-treated controls within each group, $^{**}P < 0.05$ against respective concentrations of asukamycin treatment in shControl groups in **b** and **c**, or asukamycin treatment in FLAG-GFP-expressing groups in **e**. Source data for cropped blots and bar graphs are provided.

Given the importance of PRKDC and TP53 in cancer pathogenicity, we next tested the relative contributions of these two proteins in asukamycin-mediated antiproliferative effects. TP53 knockdown, but not PRKDC knockdown, conferred complete resistance to asukamycin-mediated antiproliferative effects in 231MFP breast cancer cells, indicating that TP53 is the more critical target (Fig. 3f,g, and see Supplementary Fig. 5). Taken together, these results suggest that asukamycin has the ability to promote the formation of a gain-of-function complex between UBR7 and TP53 that results in antiproliferative effects in TNBC cell lines.

UBR7–asukamycin molecular glue interactions with TP53. We next investigated the biochemical and functional consequences of UBR7, asukamycin and TP53 interactions. We wondered whether the UBR7–asukamycin–TP53 complex might affect TP53 function in the TP53-mutant setting of TNBC cell lines. Consistent with asukamycin directly binding to TP53 and potentially stabilizing TP53 folding, asukamycin caused a significant increase in TP53 thermal stability in vitro in 231MFP cell lysate (Fig. 4a,b). We also observed a higher-molecular-mass TP53 species, which showed even greater thermal stability compared with the asukamycin-treated TP53 parental protein (Fig. 4a,b). This increased thermal stability of TP53 conferred by asukamycin was attenuated on UBR7 knockdown or FLAG–UBR7 depletion (see Extended Data Figs. 5 and 6).

Asukamycin also significantly increased TP53 binding to its DNA consensus sequence in vitro when TP53 was spiked into 231MFP cell lysate, and this increased binding was attenuated by UBR7 knockdown, indicating that asukamycin potentially activated TP53 transcriptional activity in a UBR7-dependent manner (Fig. 4c and see Extended Data Fig. 7). As other thiol-reactive compounds have been reported to both thermally stabilize TP53 and rescue the activity of mutant TP53 (ref. [29]), we next asked whether asukamycin could increase the transcriptional activity of TP53. Consistent with functional activation of p53 activity in cells, asukamycin induced the expression of the p53 target gene *TP53AIP1* in 231MFP cells. The asukamycin-mediated increase in expression was attenuated in UBR7 knockdown cells (Fig. 4d). Asukamycin also significantly induced p53 luciferase reporter transcriptional activity in HEK293T cells, even more so than the positive control topoisomerase inhibitor doxorubicin, which is known to induce apoptosis through activating the p53 pathway (Fig. 4e). This asukamycin induction of p53 transcriptional reporter activity was significantly attenuated on UBR7 knockdown or in cells expressing C374A mutant UBR7, compared with WT UBR7 in shUBR7 HEK293T cells (Fig. 4f,g, and see Extended Data Fig. 8). Consistent with asukamycin-mediated activation of p53 activity, quantitative proteomic analysis of protein expression changes, conferred by asukamycin treatment in 231MFP cells, showed that many known p53 transcriptional targets upregulated in expression, including GADD45A, GADD45B, ANKRD1, HMOX1, ATF3, PMAIP1, DDIT4, DNAJB9 and PLK2 (see Extended Data Fig. 9)[30–36]. Functional enrichment analysis of significantly upregulated proteins showed a significant enrichment in

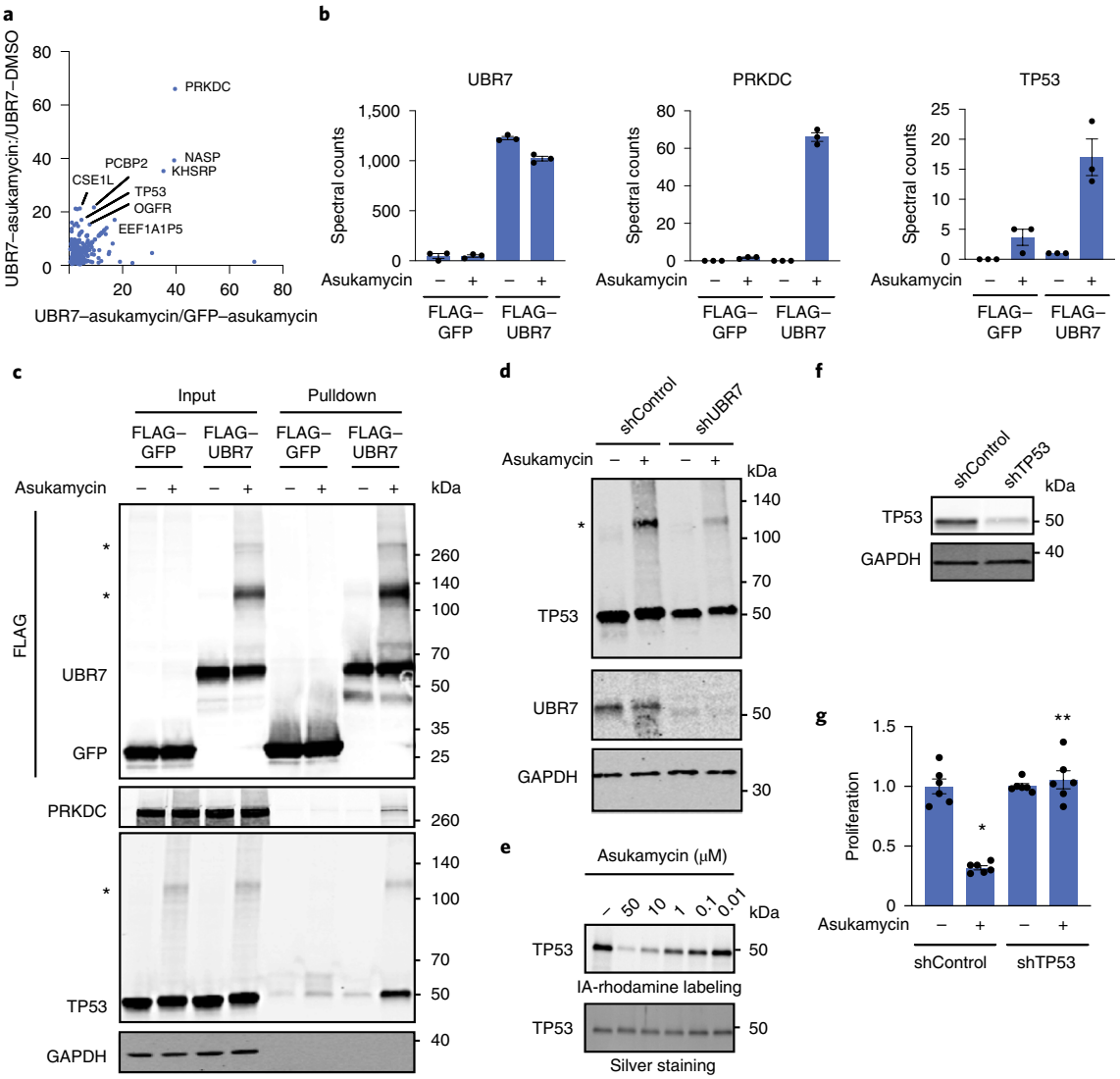

Fig. 3 | Mapping molecular glue interactions of asukamycin and UBR7. a, Proteomics analysis of molecular glue interactions of UBR7–asukamycin. The 231MFP cells stably expressing FLAG–GFP or FLAG–UBR7 were treated with DMSO or asukamycin (50 μM) for 3 h. FLAG–GFP- and FLAG–UBR7-interacting proteins were subsequently enriched and then subjected to proteomic analysis. For those proteins that showed no peptides in a particular sample group, we set them to 1, to enable relative fold-change quantification for generating this figure, and showing those proteins that showed high enrichment in asukamycin-treated FLAG–UBR7 groups compared with asukamycin-treated FLAG–GFP groups, on the *x* axis, and asukamycin-treated FLAG–UBR7 groups compared with DMSO-treated FLAG–UBR7 groups. Proteins highlighted showed >15-fold enrichment comparing UBR–asukamycin with UBR7–DMSO groups and more than a fourfold enrichment comparing UBR7–asukamycin with GFP–asukamycin groups. **b**, Spectral counts for representative proteins in the experiment described in **a**. **c**, Protein levels of FLAG-tagged proteins, PRKDC, TP53 and loading control GAPDH from a repeat of the experiment described in **a** using western blotting, showing specific interactions of PRKDC and TP53 with FLAG–UBR7 only when the cells are treated with asukamycin. Higher-molecular-mass species of FLAG–UBR7 and TP53 are noted with an asterisk (*). **d**, Anti-TP53, anti-UBR7 and loading control anti-GAPDH western blots in shControl or shUBR7 231MFP cells treated with vehicle DMSO or asukamycin (50 μM) for 3 h. A higher molecular species of TP53 is noted with an asterisk (*). Quantification for this gel is provided in Supplementary Fig. 5a**. e**, Gel-based ABPP analysis of asukamycin against pure human TP53 protein. TP53 protein was preincubated with DMSO vehicle or asukamycin for 30 min before IA-rhodamine labeling of TP53 for 1 h at room temperature. Protein was resolved by SDS–PAGE and visualized by in-gel fluorescence, and protein loading was assessed by silver staining. **f**, TP53 protein levels in 231MFP shControl and shTP53 cells. **g**, Cell proliferation of 231MFP shControl and shTP53 cells treated with DMSO or asukamycin (10 μM) for 24 h. Data shown in **b** and **g** are individual replicate values and mean ± s.e.m. ($n = 3$ for **b** and $n = 6$ for **g** biologically independent samples per group). Gels shown in **c**–**f** are representative blots from $n = 3$ biologically independent samples per group. Statistical significance was calculated using two-tailed, unpaired Student's *t*-tests and shown as: $^{*}P < 0.05$ compared with vehicle-treated controls within each group, $^{**}P < 0.05$ compared with the asukamycin-treated shControl group in **g**. Source data for cropped blots and bar graphs are provided.

the TP53 signaling pathway, as well as pathways in protein processing, senescence and mitogen-activated protein kinase signaling (see Extended Data Fig. 9). One of the well-known TP53 transcriptional tumor-suppressor targets, CDKN1A (p21), was not detected in our proteomic analysis, and thus we specifically measured CDKN1A levels and found that asukamycin significantly increased them in 231MFP cells, and that this increase was significantly attenuated on UBR7 knockdown (see Extended Data Fig. 10). We also showed that asukamycin conferred antiproliferative effects in an isogenic HCT116 colorectal cancer cell line background expressing either

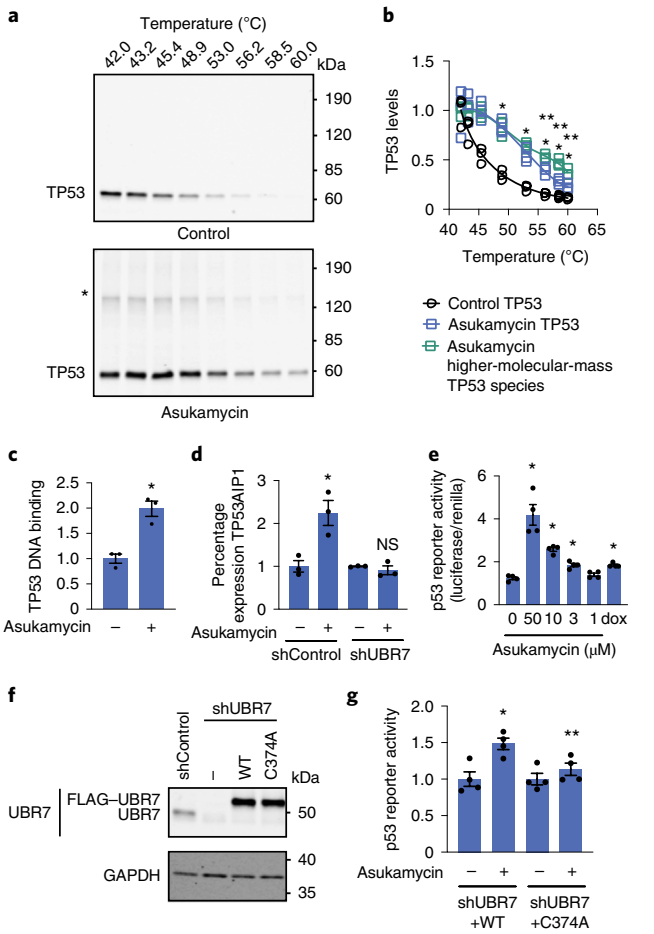

Fig. 4 | Asukamycin acts as a molecular glue between UBR7 and TP53 and activates TP53 transcriptional activity in a UBR7-dependent manner. **a**, Thermal shift assay in vitro in 231MFP breast cancer cell lysate treated with DMSO vehicle or asukamycin (50 μM). Lysate was heated to the designated temperature for 3 min, followed by 3 min at room temperature, centrifugation, and SDS–PAGE and western blotting for TP53. **b**, Quantification of TP53 parent and higher-molecular-mass levels from the thermal shift assay described in **a**. Data are normalized to respective 42 °C TP53 protein levels. **c**, TP53 DNA binding to p53 DNA consensus sequence in vitro with TP53 spiked into 231MFP breast cancer cell lysate treated with DMSO vehicle or asukamycin (50 μM). **d**, Messenger RNA expression of TP53AIP1 in 231MFP shControl and shUBR7 cells treated with DMSO vehicle or asukamycin (50 μM) for 6 h, assessed by quantitative PCR. **e**, The p53 reporter activity reported as the ratio between luciferase reporter activity versus cell number control *Renilla* levels in shUBR7 HEK293T cells expressing WT or C374A mutant UBR7, and the p53 reporter construct treated with DMSO vehicle control, asukamycin or doxorubicin (1 μM) for 6 h. **f**, Protein expression of UBR7 and loading control GAPDH in HEK293T shControl and shUBR7 cells expressing empty vector, WT UBR7 or C374A mutant UBR7 assessed using western blotting. **g**, The p53 reporter activity reported compared with DMSO vehicle-treated controls in each group in HEK293T shUBR7 cells expressing the p53 reporter construct, treated with DMSO vehicle (control) or asukamycin (10 μM) for 6 h. Data shown in **b**–**e** and **g** are individual replicate values and average ± s.e.m. ($n = 3$, for **b**–**d**, and $n = 4$, for **e** and **g**, biologically independent samples per group). Gels shown in **a** and **f** are representative blots from $n = 3$ biologically independent samples per group. Statistical significance was calculated using two-tailed, unpaired Student's *t*-tests and shown as: $^{*}P < 0.05$ compared with each temperature control group for **b**, vehicle-treated controls for **c**–**e** and **g** within each group, $^{**}P < 0.05$ compared with corresponding asukamycin treatment groups for each temperature for parent TP53 species in **b** and asukamycin-treated shUBR7 WT group in **g**. NS, not significant. Source data for cropped blots and bar graphs are provided.

the WT or the Arg 248Trp mutant TP53, but showed resistance in TP53 knockout cells (see Supplementary Fig. 6). Finally, to rule out that asukamycin was inducing TP53 transcriptional activation through DNA damage, we also demonstrated that asukamycin did not induce DNA damage compared with known DNA-damaging agents such as etoposide and hydrogen peroxide, based on the assessment of DNA damage markers such as H2A.X and RPA32 phosphorylation (see Supplementary Fig. 7).

Collectively, these results indicated that asukamycin directly targeted TP53, stabilized TP53 folding and activated p53 transcriptional activity in a UBR7 C374-dependent manner.

Activity of related natural product manumycin A. Asukamycin belongs to a larger family of polyketide natural products known as the manumycins. Although manumycin A, a close structural analog of asukamycin that also bears multiple electrophilic sites, has been shown to inhibit farnesyl transferase or sphingomyelinase[21,22] (Fig. 5a), the effect of manumycin A on UBR7 or its molecular glue activity with TP53 has not been previously reported. It is of interest that manumycin A also bound to UBR7 at a comparable potency to asukamycin by gel-based ABPP (Fig. 5b). In addition we found that manumycin A, similar to asukamycin, activated p53 transcriptional activity more so than doxorubicin (Fig. 5c). Manumycin A treatment also led to molecular glue interactions between UBR7 and TP53, and resulted in distinct higher-molecular-mass species that corresponded to the added molecular mass of TP53 and UBR7 (Fig. 5d). Finally, manumycin A, similar to asukamycin, interacted directly with TP53 by gel-based ABPP (Fig. 5e).

To investigate the relative contribution of the epoxide warhead on UBR7 binding versus TP53 binding, we prepared manumycin D (**3**) (Fig. 6a)[37], an epoxide-reduced variant, in one step from manumycin A (see Synthetic procedures)[38]. Manumycin D still labeled UBR7 by gel-based ABPP, albeit weaker than manumycin A (Fig. 6b). However, manumycin D bound less potently to TP53 compared with manumycin A or asukamycin by gel-based ABPP (Fig. 6c). Consistent with these data, manumycin D, unlike manumycin A, was incapable of inducing interactions between UBR7 and TP53 (Fig. 6d). Moreover, the antiproliferative effects and p53 transcriptional activation observed with manumycin A were attenuated with manumycin D in 231MFP breast cancer cells (Fig. 6e,f). These data collectively suggested that the epoxide contributed to interactions with TP53 and was necessary to engage in multicovalent interactions between UBR7 and TP53 to exert antiproliferative effects. These results also implied that the unsaturated side chains of manumycin A, and by analogy asukamycin, were responsible for the covalent interaction with C374 of UBR7.

Discussion

Although molecular glues are exciting therapeutic modalities that have the potential to stabilize interactions between proteins that usually would not interact, enabling exploitation of unique protein functions, the discovery of new molecular glue scaffolds has been mostly serendipitous. We postulated that natural products bearing multiple electrophilic sites may engage in multicovalent interactions that bring specific proteins into new, functionally relevant complexes. In the present study, we show that asukamycin, a manumycin polyketide bearing multiple electrophilic sites, reacts with C374 of the E3 ligase UBR7 to impair breast cancer cell proliferation through engaging in molecular glue interactions with multiple neosubstrates, including TP53. We demonstrate that asukamycin activates TP53 transcriptional activity in a UBR7 C374-dependent manner and that the antiproliferative effects observed in breast cancer cells depend on UBR7 and TP53. This molecular glue activity is also recapitulated with a related polyketide manumycin A. Furthermore, we show that manumycin D, which lacks an epoxide, still retains binding to UBR7, but shows less potent binding to TP53 and is unable to

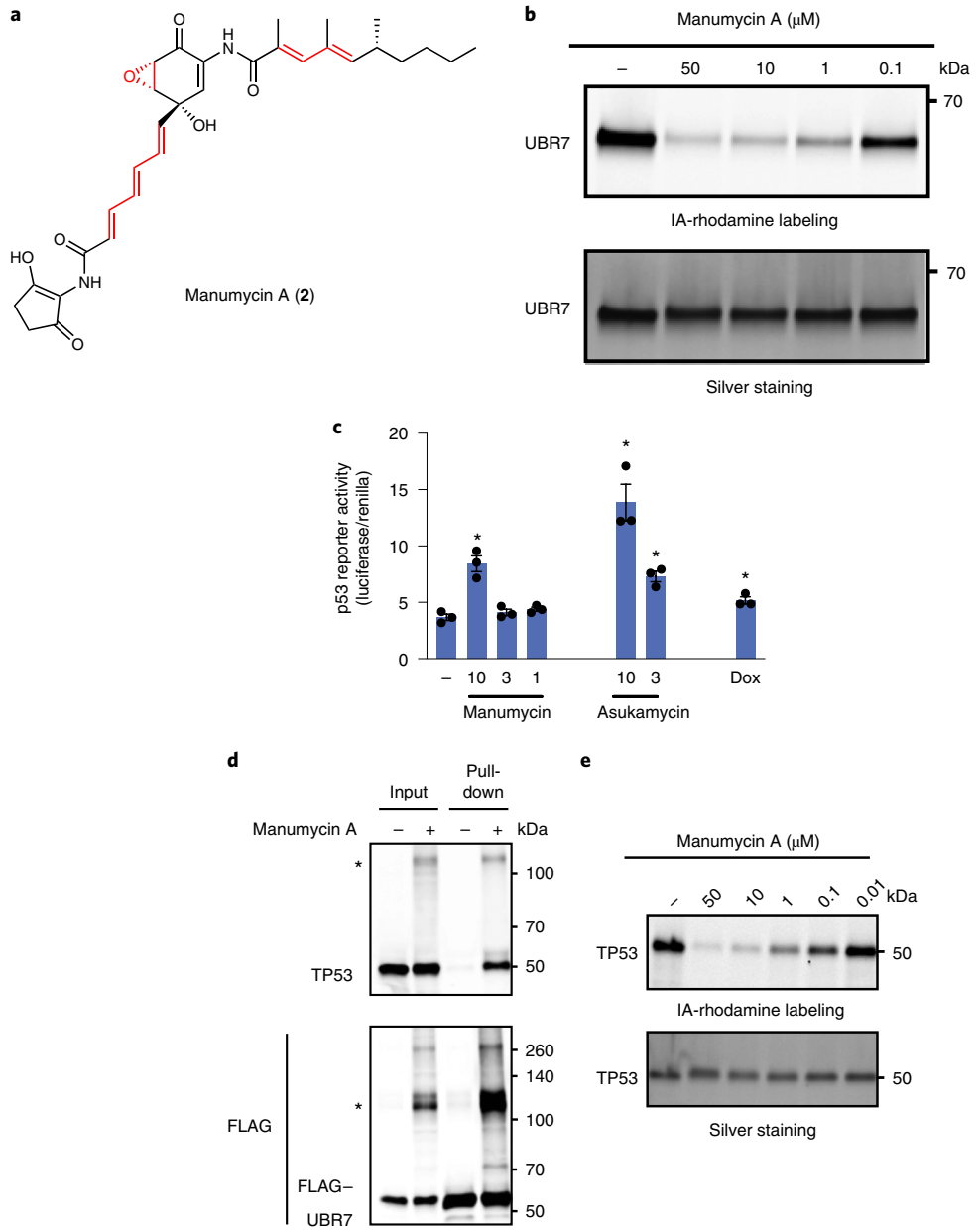

Fig. 5 | Manumycin A also interacts with UBR7 and engages in molecular glue activities with TP53. a, Structure of manumycin A highlighting potentially reactive sites in red. **b**, Gel-based ABPP analysis of manumycin A against pure human UBR7 protein. UBR7 protein was preincubated with DMSO vehicle or manumycin A for 30 min before IA-rhodamine labeling of UBR7 for 1 h at room temperature. Protein was resolved using SDS–PAGE and visualized using in-gel fluorescence, and protein loading was assessed using silver staining. **c**, The p53 reporter activity reported as the ratio between luciferase reporter activity and cell number control *Renilla* levels in HEK293T cells expressing the p53 reporter construct treated with DMSO vehicle (control), manumycin A, asukamycin or doxorubicin (1 μM) for 6 h. **d**, Protein levels of TP53 and FLAG-tagged proteins by western blotting, in 231MFP cells stably expressing FLAG–UBR7 treated with DMSO vehicle or manumycin A (50 μM) for 3 h, after which FLAG–UBR7-interacting proteins were subsequently enriched. Higher-molecular-mass TP53 and FLAG–UBR7 species are noted with an asterisk (*). **e**, Gel-based ABPP analysis of manumycin A against pure human TP53 protein. TP53 protein was preincubated with DMSO vehicle or manumycin A for 30 min before IA-rhodamine labeling of TP53 for 1 h at room temperature. Data shown in **c** are individual replicate values and mean ± s.e.m. ($n = 3$ biologically independent samples per group). Gels shown in **b**, **d** and **e** are representative blots from $n = 3$ biologically independent samples per group. Statistical significance was calculated using two-tailed, unpaired Student's *t*-tests and shown as $^*P < 0.05$ compared with vehicle-treated controls. Source data for cropped blots and bar graphs are provided.

covalently modify TP53 to the same extent, consistent with this class of molecules targeting C374 of UBR7 through a hetero-Michael addition, and then engaging TP53 probably initially through reversible binding and then through a covalent bond involving the reactive epoxide. This latter observation is based on UBR7 pulldown studies showing not only the higher-molecular-mass TP53 species, but also the parent TP53 molecular mass. Although we seem to observe one primary higher-molecular-mass UBR7-TP53 band, there were also several additional higher-molecular-mass species observed, which may correspond to multiple multicovalent interactions with the three potential reactive sites on asukamycin and manumycin A. These complexes could also contain additional molecular glue partners,

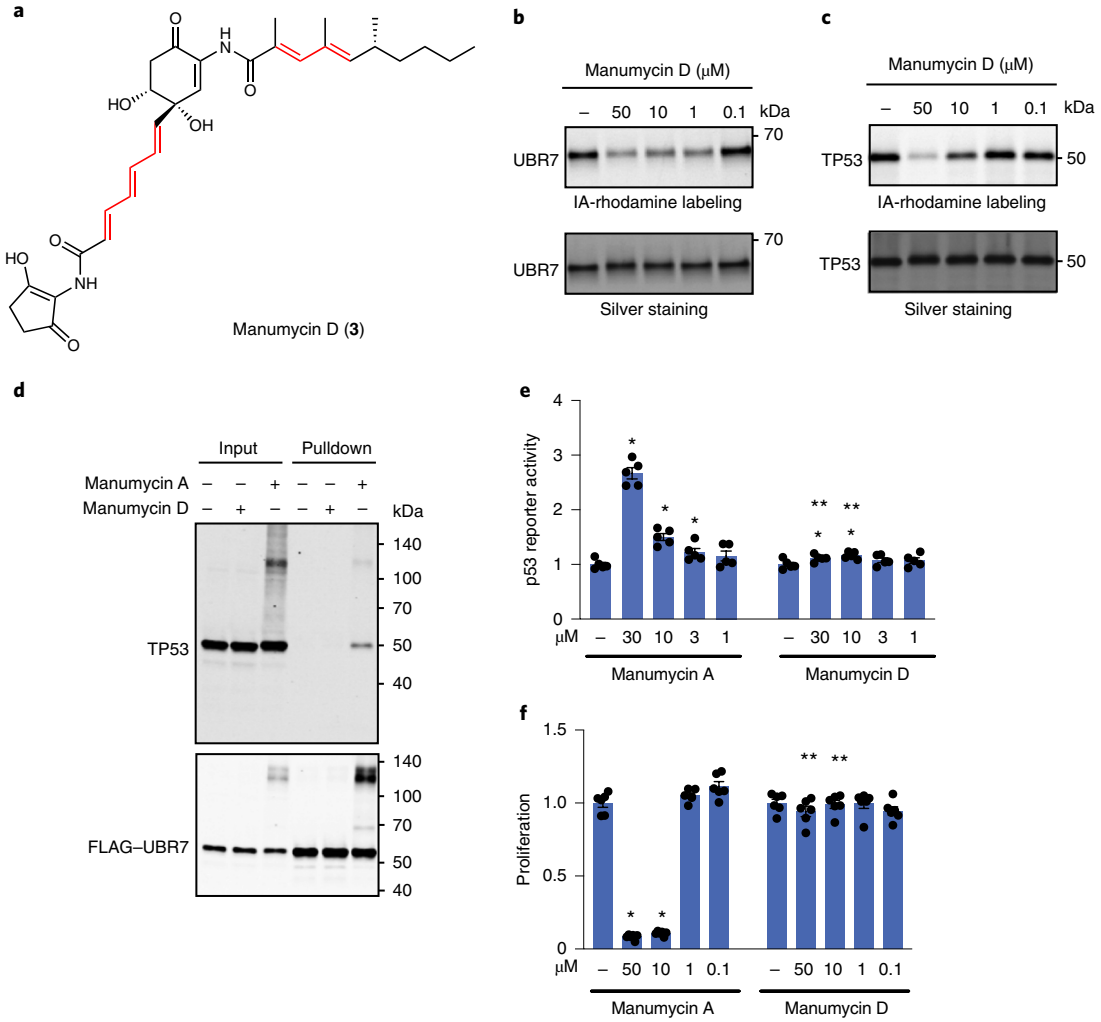

Fig. 6 | Comparing manumycin D with manumycin A. a, Structure of manumycin D with reactive sites highlighted in red. **b**, Gel-based ABPP analysis of manumycin D against pure human UBR7 protein. UBR7 protein was preincubated with DMSO vehicle or manumycin D for 30 min before IA-rhodamine labeling of UBR7 for 1 h at room temperature. **c**, Gel-based ABPP analysis of manumycin D against pure human TP53 protein. TP53 protein was preincubated with DMSO vehicle or manumycin D for 30 min before IA-rhodamine labeling of TP53 for 1 h at room temperature. **d**, Protein levels of TP53 and FLAG-tagged proteins by western blotting in 231MFP cells stably expressing FLAG–UBR7 treated with DMSO vehicle or manumycin D (50 μM) for 3 h, after which FLAG–UBR7-interacting proteins were subsequently enriched. **e**, Proliferation in 231MFP breast cancer cells treated with DMSO vehicle, manumycin A or manumycin D for 48 h and assessed by Hoechst staining. **f**, The p53 reporter activity in HEK293T cells treated with DMSO vehicle, manumycin A or manumycin D for 3 h. Gels shown in **b**–**d** are representative blots from $n = 3$ biologically independent samples per group. Data shown in **e** and **f** are individual replicate values and mean ± s.e.m. ($n = 6$, for **e**, or $n = 5$, for **f**, biologically independent samples per group). Statistical significance was calculated using two-tailed, unpaired Student's *t*-tests and shown as: $^{*}P < 0.05$ compared with vehicle-treated controls within each group and $^{**}P < 0.05$ compared with the corresponding manumycin A treatment group. Source data for cropped blots and bar graphs are provided.

such as those identified in the enrichment proteomic studies. Furthermore, although we show, using isoTOP-ABPP, that C374 of UBR7 is one of the primary targets of asukamycin and our genetic validation data show that targeting this cysteine appears to drive the asukamycin-mediated antiproliferative effects, asukamycin and manumycin A probably possess additional targets. Previously reported targets, including farnesyl transferase and sphingomyelinase, may also play a role in mediating anticancer effects or other biological activities[21,22]. Manumycin A has also been shown to interfere with IKK activity by directly binding to IKKβ and forming stable high-molecular-mass complexes, indicating that these alternate biological activities may also be mediated through additional molecular glue-type interactions beyond those reported here[39].

Several unanswered questions still remain. We do not understand how these manumycin polyketide/UBR7 complexes interact with p53 to activate p53 function. Our data suggest that the UBR7–asukamycin complex acts like a chaperone to improve TP53 thermal stability and folding, which probably improves its ability to bind to DNA and activate TP53 transcriptional activity. We also do not know the site or nature of the amino acid(s) on p53 where the suspected reaction with the epoxide takes place. We tried to map the cysteine on p53 targeted by asukamycin using liquid chromatography (LC)–MS/MS, but we were not able to detect a modified peptide, probably due to the instability of the asukamycin cysteine adduct under MS conditions. Determining which cysteine on p53 is targeted by asukamycin and is responsible for the asukamycin-mediated anticancer effects will be important for further understanding of the biological actions of asukamycin. Solving the crystal structure of the UBR7–asukamycin–TP53 ternary complex will be particularly interesting to

understand the biochemical underpinnings of this molecular glue activity. We tried to reconstitute the molecular glue activity of UBR7 with asukamycin and TP53 in vitro with purified proteins, but we observed asukamycin-mediated self-oligomerization of UBR7 and TP53 independently, which was not observed in cells or complex proteomes, further complicating in vitro biochemical and structural analysis. Furthermore, we also do not understand the endogenous role of UBR7 and whether asukamycin affects this function. UBR7 belongs to the UBR family of *N*-recognin E3 ligases, but, unlike UBR1-6, contains a plant homeodomain rather than an F-box domain[40]. It has been reported that UBR7 can ubiquitinylate histones and has a variety of interacting partners in other contexts[41]. Our data currently suggest that the asukamycin-mediated phenotypes and effects on TP53 activity are independent of ubiquitination functions of UBR7. However, we cannot exclude the normal functional role of UBR7 in conferring the anticancer activity of asukamycin[26,41]. Previous studies have suggested that UBR7 functions as a tumor suppressor in TNBC cells[26], through reducing monoubiquitination of histone H2B and reducing CDH4 levels, but our proteomic profiling studies show that asukamycin does not affect CDH4 expression (see Extended Data Fig. 9) and asukamycin broadly impairs TNBC cell growth, further indicating that asukamycin confers a gain of function to UBR7, independent of its potential endogenous role. Further work will be critical for a better understanding of the role of UBR7 and cancer.

Despite these remaining questions, our study showcases the possibility that multicovalent small molecules can potentially act as new molecular glues, and that these interactions can be quickly deciphered using chemoproteomic approaches. Of future interest will be whether other natural products or synthetic small molecules that bear multiple reactive centers can act as specific molecular glues to confer new protein functions. In addition, the ability of manumycin polyketides to template the interaction of UBR7 with multiple other proteins warrants the further examination of this family of natural products for applications beyond cancer. Quite intriguingly, unsaturated side chains reminiscent of the manumycins appear in many other natural products, many of which also harbor diverse electrophilic warheads[42–44]. Moreover, the multitude of polycyclic natural products containing one or more potentially protein-reactive functional groups is vast, implying that this concept might extend across a greater section of natural product space[45,46].

Online content

Any Nature Research reporting summaries, source data, extended data, supplementary information, acknowledgements, peer review information; details of author contributions and competing interests; and statements of data and code availability are available at https://doi.org/10.1038/s41589-020-0557-2.

Received: 21 October 2019; Accepted: 29 April 2020;
Published online: 22 June 2020

References

1. Roberts, A. M., Ward, C. C. & Nomura, D. K. Activity-based protein profiling for mapping and pharmacologically interrogating proteome-wide ligandable hotspots. *Curr. Opin. Biotechnol.* **43**, 25–33 (2017).
2. Backus, K. M. et al. Proteome-wide covalent ligand discovery in native biological systems. *Nature* **534**, 570–574 (2016).
3. Burslem, G. M. & Crews, C. M. Small-molecule modulation of protein homeostasis. *Chem. Rev.* **117**, 11269–11301 (2017).
4. Hughes, S. J. & Ciulli, A. Molecular recognition of ternary complexes: a new dimension in the structure-guided design of chemical degraders. *Essays Biochem* **61**, 505–516 (2017).
5. Andrei, S. A. et al. Stabilization of protein-protein interactions in drug discovery. *Expert Opin. Drug Discov* **12**, 925–940 (2017).
6. Milroy, L.-G., Grossmann, T. N., Hennig, S., Brunsveld, L. & Ottmann, C. Modulators of protein-protein interactions. *Chem. Rev.* **114**, 4695–4748 (2014).
7. Schreiber, S. L. Chemistry and biology of the immunophilins and their immunosuppressive ligands. *Science* **251**, 283–287 (1991).
8. Ottmann, C. et al. A structural rationale for selective stabilization of anti-tumor interactions of 14-3-3 proteins by cotylenin A. *J. Mol. Biol.* **386**, 913–919 (2009).
9. Lu, G. et al. The myeloma drug lenalidomide promotes the cereblon-dependent destruction of Ikaros proteins. *Science* **343**, 305–309 (2014).
10. Chamberlain, P. P. et al. Structure of the human Cereblon-DDB1-lenalidomide complex reveals basis for responsiveness to thalidomide analogs. *Nat. Struct. Mol. Biol.* **21**, 803–809 (2014).
11. Matyskiela, M. E. et al. SALL4 mediates teratogenicity as a thalidomide-dependent cereblon substrate. *Nat. Chem. Biol.* **14**, 981–987 (2018).
12. Donovan, K. A. et al. Thalidomide promotes degradation of SALL4, a transcription factor implicated in Duane Radial Ray Syndrome. *eLife* **7**, e38430 (2018).
13. Guo, Z. et al. Rapamycin-inspired macrocycles with new target specificity. *Nat. Chem.* **11**, 254 (2019).
14. Sievers, Q. L. et al. Defining the human C2H2 zinc finger degrome targeted by thalidomide analogs through CRBN. *Science* **362**, eaat0572 (2018).
15. Lagoutte, R. & Winssinger, N. Following the lead from nature with covalent inhibitors. *Chimia* **71**, 703–711 (2017).
16. Weerapana, E. et al. Quantitative reactivity profiling predicts functional cysteines in proteomes. *Nature* **468**, 790–795 (2010).
17. Sattler, I., Thiericke, R. & Zeeck, A. The manumycin-group metabolites. *Nat. Prod. Rep.* **15**, 221–240 (1998).
18. Omura, S., Kitao, C., Tanaka, H., Oiwa, R. & Takahashi, Y. A new antibiotic, asukamycin, produced by *Streptomyces*. *J. Antibiot.* **29**, 876–881 (1976).
19. Hu, Y. & Floss, H. G. New type II manumycins produced by *Streptomyces nodosus* ssp. *asukaensis* and their biosynthesis. *J. Antibiot.* **54**, 340–348 (2001).
20. Shipley, P. R., Donnelly, C. C. A., Le, C. H., Bernauer, A. D. & Klegeris, A. Antitumor activity of asukamycin, a secondary metabolite from the actinomycete bacterium *Streptomyces nodosus* subspecies *asukaensis*. *Int. J. Mol. Med.* **24**, 711–715 (2009).
21. Arenz, C. et al. Manumycin A and its analogues are irreversible inhibitors of neutral sphingomyelinase. *Chembiochem. Eur. J. Chem. Biol.* **2**, 141–143 (2001).
22. Hara, M. et al. Identification of Ras farnesyltransferase inhibitors by microbial screening. *Proc. Natl Acad. Sci. USA* **90**, 2281–2285 (1993).
23. Bianchini, G., Balko, J. M., Mayer, I. A., Sanders, M. E. & Gianni, L. Triple-negative breast cancer: challenges and opportunities of a heterogeneous disease. *Nat. Rev. Clin. Oncol.* **13**, 674–690 (2016).
24. Kozawa, I., Kato, K., Teruya, T., Suenaga, K. & Umezawa, K. Unusual intramolecular N->O acyl group migration occurring during conjugation of (–)-DHMEQ with cysteine. *Bioorg. Med. Chem. Lett.* **19**, 5380–5382 (2009).
25. Spradlin, J. N. et al. Harnessing the anti-cancer natural product nimbolide for targeted protein degradation. *Nat. Chem. Biol.* **15**, 747–755 (2019).
26. Adhikary, S. et al. Atypical plant homeodomain of UBR7 functions as an H2BK120Ub ligase and breast tumor suppressor. *Nat. Commun.* **10**, 1398 (2019).
27. Goodwin, J. F. & Knudsen, K. E. Beyond DNA repair: DNA-PK function in cancer. *Cancer Discov* **4**, 1126–1139 (2014).
28. Levine, A. J. & Oren, M. The first 30 years of p53: growing ever more complex. *Nat. Rev. Cancer* **9**, 749–758 (2009).
29. Zhang, Q., Bergman, J., Wiman, K. G. & Bykov, V. J. N. Role of thiol reactivity for targeting mutant p53. *Cell Chem. Biol.* **25**, 1219–1230.e3 (2018).
30. Zhan, Q. Gadd45a, a p53- and BRCA1-regulated stress protein, in cellular response to DNA damage. *Mutat. Res.* **569**, 133–143 (2005).
31. Kim, Y.-A. et al. Gadd45β is transcriptionally activated by p53 via p38α-mediated phosphorylation during myocardial ischemic injury. *J. Mol. Med. Berl. Ger* **91**, 1303–1313 (2013).
32. Fan, F. et al. ATF3 induction following DNA damage is regulated by distinct signaling pathways and over-expression of ATF3 protein suppresses cells growth. *Oncogene* **21**, 7488–7496 (2002).
33. Oda, E. et al. Noxa, a BH3-only member of the Bcl-2 family and candidate mediator of p53-induced apoptosis. *Science* **288**, 1053–1058 (2000).
34. Du, F. et al. DDIT4 promotes gastric cancer proliferation and tumorigenesis through the p53 and MAPK pathways. *Cancer Commun.* **38**, 45 (2018).
35. Lee, H. J. et al. Genotoxic stress/p53-induced DNAJB9 inhibits the pro-apoptotic function of p53. *Cell Death Differ.* **22**, 86–95 (2015).
36. Matthew, E. M. et al. The p53 target Plk2 interacts with TSC proteins impacting mTOR signaling, tumor growth and chemosensitivity under hypoxic conditions. *Cell Cycle* **8**, 4168–4175 (2009).
37. Kohno, J. et al. TMC-1 A, B, C and D, new antibiotics of the manumycin group produced by *Streptomyces* sp. Taxonomy, production, isolation, physico-chemical properties, structure elucidation and biological properties. *J. Antibiot.* **49**, 1212–1220 (1996).

38. Grové, J. J. C., Wei, X. & Taylor, R. J. K. The first total synthesis of a type II manumycin antibiotic, (+)-TMC-1 A: the total syntheses of (–)-LL-C10037β and (+)-manumycin B. *Chem. Commun*. **5**, 421–422 (1999).
39. Bernier, M. et al. Binding of manumycin A inhibits IkappaB kinase beta activity. *J. Biol. Chem*. **281**, 2551–2561 (2006).
40. Tasaki, T. et al. The substrate recognition domains of the N-end rule pathway. *J. Biol. Chem*. **284**, 1884–1895 (2009).
41. Kleiner, R. E., Hang, L. E., Molloy, K. R., Chait, B. T. & Kapoor, T. M. A chemical proteomics approach to reveal direct protein–protein interactions in living cells. *Cell Chem. Biol.* **25**, 110–120.e3 (2018).
42. Haritakun, R., Srikitikulchai, P., Khoyaiklang, P. & Isaka, M. Isariotins A–D, alkaloids from the insect pathogenic fungus *Isaria tenuipes* BCC 7831. *J. Nat. Prod.* **70**, 1478–1480 (2007).
43. Hammerschmidt, L. et al. Cytotoxic acyl amides from the soil fungus *Gymnascella dankaliensis*. *Bioorg. Med. Chem.* **23**, 712–719 (2015).
44. Amagata, T., Minoura, K. & Numata, A. Gymnastatins F–H, cytostatic metabolites from the sponge-derived fungus *Gymnascella dankaliensis*. *J. Nat. Prod.* **69**, 1384–1388 (2006).
45. Gersch, M., Kreuzer, J. & Sieber, S. A. Electrophilic natural products and their biological targets. *Nat. Prod. Rep.* **29**, 659–682 (2012).
46. Zeng, T. et al. Exploring chemical and biological space of terpenoids. *J. Chem. Inf. Model.* **59**, 3667–3678 (2019).

Methods

Materials. Asukamycin and manumycin A were obtained from Cayman Chemicals and were >95% pure. Heavy and light tobacco etch virus (TEV)–biotin tags were synthesized according to previously described methods[16]. Manumycin D synthesis and characterization are shown in Synthetic procedures. Recombinant UBR7 pure proteins were purchased from Origene or NOVUS Biologicals. Recombinant TP53 pure protein was purchased from R&D Systems.

Cell culture. The 231MFP cells were obtained from Professor B. Cravatt and were generated from explanted tumor xenografts of MDA-MB-231 cells as previously described[47]. HCC38 and HEK293T cells were obtained from the American Type Culture Collection. Isogenic HCT116 colorectal cancer cell lines were generated by Novartis. The 231MFP cells were cultured in L15 medium (HyClone) containing 10% fetal bovine serum (FBS) and 2 mM glutamine, and maintained at 37 °C with 0% CO_2. HEK293T and isogenic HCT116 cell lines cells were cultured in Dulbecco's modified Eagle's medium containing 10% FBS and 2 mM glutamine, and maintained at 37 °C with 5% CO_2. HCC38 cells were cultured in RPMI medium containing 10% FBS and maintained at 37 °C with 5% CO_2.

Survival and proliferation assays. Cell survival and proliferation studies were performed using Hoechst 33342 dye (Invitrogen) as described previously[25]. Briefly, 231MFP cells were seeded at 20,000 (proliferation) or 40,000 (survival) cells per well, respectively, in serum-containing (proliferation) or serum-free (survival) medium in 96-well plates, and allowed to adhere overnight. Under serum-free survival conditions, we have previously observed that the cells do not proliferate, and thus we are measuring loss of viability in these cells under serum-free conditions with pharmacological treatment[48]. Under serum-containing conditions, the cells proliferate normally, and thus pharmacological effects in this assay indicate a combination of loss of proliferation and viability. The cells were treated with dimethyl sulfoxide (DMSO) vehicle- or asukamycin-containing medium for 24 or 48 h before fixation, and stained with 10% formalin and Hoechst 33342 dye. Studies with HCC38 cells were also performed as above, but were seeded with 10,000 cells per well for proliferation and 20,000 cells per well for survival.

Growth inhibition assay across cancer cell line panel. Cells in growth medium were plated into a 1,536-well plate (5 µl per well, 250 cells per well) using a GNF Bottle Valve liquid handler. A Labcyte Echo acoustic transfer instrument was used to transfer 15 nl of compounds in DMSO to each well (final concentration 30, 9.5, 3, 1, 0.3, 0.1, 0.03 and 0.01 µM). The cells were then incubated (37 °C, 95% humidity, 5% CO_2) for 3 d and 6 h before the addition of 4 µl of 50% Cell-Titer Glo (Promega) in water using a GNF Bottle Valve liquid handler. Plates were incubated with Cell Titer Glo for 15 min at room temperature before reading the luminescence (5 s exposure) on a Perkin Elmer ViewLux. For determining GI_{50} values, data were normalized to a day 0 cell count, measured using a cell plate copy that was not treated with compound, and growth inhibition dose–response curves were calculated using Helios.

IsoTOP-ABPP of asukamycin targets. IsoTOP-ABPP studies were done as previously reported[25]. The 231MFP cells were treated with DMSO vehicle or 10 µM asukamycin for 3 h. Cells were then harvested and lysed by probe sonication in phosphate-buffered saline (PBS) and protein concentrations were determined by bicinchoninic acid (BCA) assay (Pierce). Proteomes were subsequently labeled with 100 µM IA-alkyne (CHESS Gmbh) at room temperature for 1 h. Copper-catalyzed, azide–alkyne cycloaddition (CuAAC) was performed by sequential addition of tris(2-carboxyethyl)phosphine (TCEP, 1 mM, Sigma), tris((1-benzyl-1H-1,2,3-triazol-4-yl)methyl(amine (34 mM, Sigma), copper (II) sulfate (1 mM, Sigma) and biotin-linker-azide, the linker functionalized with a TEV protease recognition sequence, along with an isotopically light or heavy valine for treatment of vehicle- or asukamycin-treated proteome, respectively. After CuAAC, proteomes were precipitated by centrifugation at 6,500*g*, washed in ice-cold methanol, combined in a 1:1 vehicle:asukamycin ratio, washed again, then denatured and resolubilized by heating in 1.2% SDS/PBS at 80 °C for 5 min. Insoluble components were precipitated by centrifugation at 6,500*g* and soluble proteome was diluted with PBS to make 0.2% SDS. Labeled proteins were bound to streptavidin–agarose beads (Pierce) while rotating overnight at 4 °C. After washing three times each in PBS and water, the bead-linked proteins were resuspended in 6 M urea/PBS and reduced in 1 mM TCEP, alkylated with 18 mM IA (Sigma), then washed and resuspended in 2 M urea and trypsinized overnight at 37 °C, with 2 µg per sample sequencing grade trypsin (Promega). After washing three times each in PBS and water, the beads were resuspended in TEV buffer solution (1× TEV buffer containing 100 µM dithiothreitol) and incubated overnight at 29 °C with AcTEV Protease (Invitrogen). Peptides were diluted in water and acidified with 1.2 M formic acid (Spectrum) for isoTOP-ABPP analysis. Subsequent steps of the isoTOP-ABPP and MA analysis were performed using the same methods as we have described previously[25].

Data were extracted in the form of MS1 and MS2 files using Raw Extractor v.1.9.9.2 (Scripps Research Institute) and searched against the Uniprot human database using ProLuCID search methodology in IP2 v.3 (Integrated Proteomics Applications, Inc.)[49]. Cysteine residues were searched with a static modification for carboxyaminomethylation (+57.02146), and up to two differential modifications for methionine oxidation and either the light or the heavy TEV tags (+464.28596 or +470.29977, respectively). Peptides were required to be fully tryptic peptides and to contain the TEV modification. ProLUCID data were filtered through DTASelect to achieve a peptide false-positive rate <5%. Only those probe-modified peptides that were evident across two out of three biological replicates were interpreted for their isotopic light:heavy ratios. For those probe-modified peptides that showed ratios >2, we interpreted only those targets that were present across all three biological replicates, were statistically significant and showed good quality MS1 peak shapes across all biological replicates. Light versus heavy isotopic probe-modified peptide ratios are calculated by taking the mean of the ratios of each replicate paired light versus heavy precursor abundance for all peptide spectral matches associated with a peptide. The paired abundances were also used to calculate a paired-sample *t*-test *P* value in an effort to estimate constancy within paired abundances and significance in change between treatment and control. *P* values were corrected using the Benjamini–Hochberg method. Data processing and statistical analysis algorithms from our lab can be found on our lab's Github site: https://github.com/NomuraRG, and we can make any further code from the present study available on reasonable request.

Gel-based ABPP. Recombinant pure protein (0.1 µg per sample) was pretreated with either DMSO vehicle or natural products at 37 °C for 30 min in 25 µl PBS, and subsequently treated with 200 nM IA-rhodamine (Setareh Biotech) at room temperature for 1 h. The reaction was stopped by addition of 4× reducing Laemmli SDS sample loading buffer (Alfa Aesar). After boiling at 95 °C for 5 min, the samples were separated on precast 4–20% Criterion TGX gels (Bio-Rad). Probe-labeled proteins were analyzed by in-gel fluorescence using a ChemiDoc MP (Bio-Rad).

Constructing knockdown lines and reinforced expression or overexpression lines. Short-hairpin oligonucleotides were used to knock down the expression of UBR7 or TP53 in 231MFP cells using previously described methods[25]. For lentivirus production, lentiviral plasmids and packaging plasmids (pMD2.5G, Addgene catalog no. 12259 and psPAX2, Addgene catalog no. 12260) were transfected into HEK293T cells using Lipofectamine 2000 (Invitrogen). Lentivirus was collected from filtered cultured medium and used to infect the target cell line with 1:1,000 dilution of polybrene. Target cells were selected over 3 d with 1 µg ml^{-1} of puromycin. The short-hairpin sequences which were used for generation of the knockdown lines were:

UBR7: CCGGGATGATGTCCGGGAGGTTAAACTCGAGTTTAACCT-CCCGGACATCATCTTTTTG (Sigma UBR7 MISSION shRNA Bacterial Glycerol Stock, TRCN0000294293).
TP53: CCGGCGGCGCACAGAGGAAGAGAATCTCGAGATTCTC-TTCCTCTGTGCGCCGTTTTT (Sigma TP53 MISSION shRNA Bacterial Glycerol Stock, TRCN0000003753).
PRKDC:
CCGGCCTGAAGTCTTTACAACATATCTCGAGATATGTTGTAAAGACTT CAGGTTTTTTG (Sigma PRKDC MISSION shRNA Bacterial Glycerol Stock, TRCN0000194719).
MISSION TRC1.5 pLKO.1- or TRC2 pLKO.5-puro Non-Mammalian shRNA Control (Sigma) was used as a control shRNA.

For expression of WT or C374A mutant UBR7 on UBR7 knockdown, cells were transiently transfected with a UBR7 expression plasmid using Lipofectamine 2000. WT human UBR7 expression plasmid with a C-terminal FLAG tag was purchased from Origene (catalog no. RC218298). The UBR7 C374A mutant was generated with Q5 Site-Directed Mutagenesis Kit (New England Biolabs) according to the manufacturer's protocols.

For making stable overexpression lines, lentivirus was used as with the knockdown lines described above. To make lentiviral constructs for GFP and UBR7, Gibson assembly was performed using a Gibson Assembly Cloning Kit (New England Biolabs) according to the manufacturer's protocols. The primer sequences that were used to amplify the open reading frames with desired overlaps, or to linearize the pLenti-Entry backbone (PS100069, Origene), were:

GFP forward: GCCGCCGCGATCGCCatggtgagcaagggcgagg
GFP reverse: CGGCCGCGTACGCGTcttgtacagctcgtccatgc
UBR7 forward: GCCGCCGCGATCGCCatggccggagccgagggcg
UBR7 reverse: CGGCCGCGTACGCGTgctgcagtaatactgcatcg
pLenti-Entry forward: ACGCGTACGCGGCCGCTCGAG
pLenti-Entry reverse: GGCGATCGCGGCGGCAGATC

For transient knockdown of UBR7 with small interfering (si)RNA (Dharmacon), cells were seeded in six-well plates overnight (200,000 cells per well for 231MFP cells and 300,000 cells per well for HEK293T cells) and then transfected with either non-targeting siRNA oligonucleotide (siControl, Dharmacon, catalog no. D-001810-01) or siUBR7 oligonucleotides (Dharmacon, catalog no. J-016489-11) using Dharmafect 1 (Dharmacon). Cells were harvested 48 h after transfection for seeding for luciferase reporter assays, or treated with DMSO vehicle or asukamycin 72 h after transfection to see protein expression by western blotting.

Western blotting. FLAG antibody (M2) was obtained from Sigma. Antibodies to UBR7 (PA5-31559) and p53 (DO-1) were obtained from Thermo Fisher Scientific.

Antibodies to GAPDH (D16H11), ubiquitin (P4D1), FLAG (D6W5B), p21 (12D1), histone H2A II (2578S), p-histone H2A.X (2577S), RPA32 (4E4) and p-RPA32/RPA2 (83745S) were obtained from Cell Signaling Technology.

Proteins were resolved by SDS–PAGE and transferred to nitrocellulose membranes using the iBlot system (Invitrogen). Membranes were blocked with 5% nonfat milk or bovine serum albumin in Tris-buffered saline (TBS) containing Tween 20 (TBS-T) solution for 30 min at room temperature, washed in TBS-T, and probed with primary antibody diluted in recommended diluent per manufacturer overnight at 4 °C. After three washes with TBS-T, the membranes were incubated in the dark with IR800-conjugated secondary antibodies at 1:10,000 dilution in 5% nonfat milk in TBS-T at room temperature for 1 h. Blots were visualized using an Odyssey Li-Cor fluorescent scanner. The membranes were stripped using ReBlot Plus Strong Antibody Stripping Solution (EMD Millipore), when additional primary antibody incubations were performed. For dual-color western blotting, anti-mouse IR680 and anti-rabbit IR800 were used to detect TP53 (DO-1) and FLAG (D6W5B), respectively.

Quantitative PCR. Total RNA was extracted from cultured cells with TRIzol reagent (Thermo Fisher Scientific), and complementary DNA was synthesized using the Maxima Reverse Transcriptase (Thermo Fisher Scientific). Gene expression was measured from the cDNA using DyNAmo HS SYBR Green qPCR Kit (Thermo Fisher Scientific) on a Bio-Rad CFX Connect PCR system. Samples were measured in technical triplicate, and PRKDC expression was normalized to GAPDH levels and calculated using the comparative Ct method. The following primer sequences were used for quantitative PCR:

PRKDC forward: CTGTGCAACTTCACTAAGTCCA
PRKDC reverse: CAATCTGAGGACGAATTGCCT
GAPDH forward: GGAGCGAGATCCCTCCAAAAT
GAPDH reverse: GGCTGTTGTCATACTTCTCATGG.

Anti-FLAG pulldown. The 231MFP cells with stable expression of FLAG–GFP or FLAG–UBR7 were treated with DMSO vehicle or 50 µM asukamycin for 3 h. Cells were collected, washed twice with PBS and lysed by probe sonication in TBS. After centrifugation at 12,000*g* for 10 min, the supernatant was incubated with Anti-DYKDDDDK G1 affinity resin (GenScript) at 4 °C for 3 h. Beads were washed twice with 1 ml cold TBS (10 min per incubation), and the samples were eluted twice by 250 µg ml^{-1} of 3× FLAG–peptide solution. Eluent was subsequently prepared for proteomic analysis as described under Proteomic analysis of pulldown samples.

Proteomic analysis of pulldown samples. The samples were precipitated by addition of trichloroacetic acid at a final concentration of 20% and incubated at −80 °C for 1 h. The samples were then centrifuged at 14,800*g* for 10 min and supernatant was carefully removed. After washing twice with ice-cold 0.01 M HCl/90% acetone solution, the precipitated protein was resuspended in 4 M urea containing 0.1% Protease Max (Promega) and diluted in 40 mM ammonium bicarbonate buffer. The samples were reduced with 10 mM TCEP at 60 °C for 30 min. The samples were then diluted with PBS and incubated overnight at 37 °C with sequencing-grade trypsin. After centrifugation at 13,200*g* for 30 min, the supernatant was acidified with 5% formic acid and subsequently analyzed by LC–MS/MS. Data were analyzed by spectral counting. Only those proteins that showed more than two peptides in at least one sample were subsequently interpreted. Although this filtered and original list was interpreted for mean, s.e.m. and *P* values, for visual representation of these proteomic data in Fig. 3a, we set those proteins that showed averages <1 within a particular group as 1 to generate fold-changes that could be plotted in the figure.

In-gel digestion of higher-molecular-mass region for pulldown products. Products from anti-FLAG pulldown were resolved by 4–20% SDS–PAGE using Tris–Glycine precast Mini-PROTEAN TGX gel (Bio-Rad). The molecular-mass region between 100 and 140 kDa was excised from the gel. Samples were then reduced, alkylated and tryptically digested in-gel as previously described[50].

Tryptic peptides were analyzed using a Q-Exactive Plus mass spectrometer using the same method as for isoTOP-ABPP.

FLAG–UBR7 immunodepletion. The 231MFP cells with stable expression of FLAG–UBR7 were washed twice with PBS, and lysed by probe sonication in TBS containing a protease inhibitor cocktail (Pierce), and protein concentrations were determined by BCA assay. Cell lysates (1 mg ml^{-1}) were incubated with FLAG antibody (Sigma, M2, 20 µg) on ice for 1 h. Subsequently samples were incubated with 100 µl Pierce Protein G Agarose (Pierce) by rotating overnight at 4 °C. Samples were centrifuged, and the unbound supernatant was collected for thermal shift assay.

In vitro deubiquitination assay. The 231MFP cells were treated with either DMSO vehicle or 50 µM asukamycin for 3 h. Cells were then harvested and lysed by probe sonication in TBS, and protein concentrations were determined by BCA assay. Cell lysates were incubated with deubiquitinating enzyme USP2 (R&D Systems) at 37 °C for 1 h. The reaction was stopped by addition of 4× reducing Laemmli SDS sample loading buffer. The reaction products were analyzed using western blotting.

Thermal shift assay. The 231MFP cells were lysed by probe sonication in TBS containing a complete protease inhibitor cocktail (Roche), and protein concentrations were determined by BCA assay. Cell lysates (1 mg ml^{-1}) were treated with either DMSO vehicle or 50 µM asukamycin for 1 h at 37 °C. Cell lysates were then separated into eight fractions for thermal profiling. Fractions were heated at the indicated temperatures (42–60 °C) for 3 min using a thermal cycler (T100 Thermal Cycler, Bio-Rad), followed by 3 min at room temperature. Samples were then centrifuged at 16,000*g* for 15 min to separate protein aggregates from soluble proteins. Supernatants were collected and analyzed by western blotting.

In vitro transcription factor assay for TP53. Recombinant TP53 protein (0.05 µg per sample) was spiked into 40 µl 231MFP breast cancer cell lysate (0.5 mg ml^{-1} in TBS) and then treated with either DMSO vehicle or 50 µM asukamycin for 1 h at 37 °C. TP53 DNA binding to the p53 DNA consensus sequence was then assessed using the p53 transcription factor assay kit (Cayman) according to the manufacturer's protocols.

Luciferase reporter assay. HEK293T cells were seeded at 30,000 cell per well in 96-well plates. After 24 h, the cells were transiently co-transfected with 0.1 µg per well of pGL4.38 (luc2P/p53 RE/Hygro) (Promega) and 0.02 µg per well of pRL-TK (*Renilla* luciferase control vector) using Lipofectamine 2000. After treating the cells with compounds for 6 h, the expression levels of the firefly and *Renilla* luciferase reporter genes were examined using a Dual-Glo luciferase assay system (Promega) according to the manufacturer's protocols. The luminescent signals were measured using a SpectraMax i3 plate reader (Molecular Devices).

LC–MS/MS analysis of intracellular asukamycin level. The 231MFP cells were seeded at 1,000,000 cells per dish in serum-containing L15 medium in 6-cm dishes and allowed to adhere overnight. The medium was than replaced with serum-containing or serum-free L15 containing DMSO or asukamycin. After 1.5 h cells were washed twice with PBS, and asukamycin was extracted from the cells using a chloroform:methanol:PBS solution mixture (2:1:1, v/v/v; 4 ml total), with 3-*O*-dodecyl-*sn*-glycerol (10 nmol, Santa Cruz Biotechnology) as an internal standard. The organic layer was collected, evaporated under a stream of N_2, resolubilized in chloroform and analyzed by multiple-reaction, monitoring-based targeted LC–MS/MS on an Agilent 6430 QQQ using a Luna reverse-phase C5 column (50 × 4.6 mm^2 with particles of 5-mm diameter, Phenomenex) as described previously[51]. Parent/daughter ion, multiple-reaction monitoring transitions used to determine asukamycin levels were 547.2/189.2, with a collision energy of 15 V. The peak area of asukamycin to that of internal standard was determined.

Quantitative TMT proteomics analysis. Quantitative tandem mass tag (TMT)-based proteomics analysis was performed as previously described[25]. Acquired MS data were processed using Proteome Discoverer v.2.2.0.388 software (Thermo) using Mascot v.2.5.1 search engine (Matrix Science) together with Percolator validation node for peptide–spectral match filtering[52]. Data were searched against the Uniprot protein database (canonical human and mouse sequences) supplemented with sequences of common contaminants. Peptide search tolerances were set to 10 ppm for precursors and 0.8 Da for fragments. Trypsin cleavage specificity (cleavage at lysine, arginine except if followed by proline) allowed for up to two missed cleavages. Carbamidomethylation of cysteine was set as a fixed modification, methionine oxidation and TMT modification of N-termini, and lysine residues were set as variable modifications. Data validation of peptide and protein identifications was done at the level of the complete dataset, consisting of combined Mascot search results for all individual samples per experiment via the Percolator validation node in Proteome Discoverer. Reporter ion ratio calculations were performed using summed abundances with the most confident centroid selected from the 20-ppm window. Only peptide–spectrum matches that are unique assignments to a given identified protein within the total dataset are considered for protein quantitation. High confidence protein identifications were reported using a Percolator-estimated <1% false discovery rate cut-off. Differential abundance significance was estimated using a background-based analysis of variance with Benjamini–Hochberg correction to determine adjusted *P* values.

Gene enrichment analysis was performed using gProfiler. Statistical analysis was performed using the g:SCS algorithm for computing multiple testing correction for *P* values gained from Gene Ontology and pathway enrichment analysis. It corresponds to an experiment-wide threshold of $a = 0.05$. Given a fixed input query size, g:SCS analytically approximates a threshold t corresponding to the 5% upper quantile of randomly generated queries of that size. All actual *P* values resulting from the query are transformed to corrected *P* values by multiplying these by the ratio of the approximate threshold t and the initial experiment-wide threshold $a = 0.05$ (refs. [53–55]).

Reporting summary. Further information on research design is available in the Nature Research Reporting Summary linked to this article.

Data availability

The datasets generated during and/or analyzed during the current study are available from the corresponding author on reasonable request. Source data for Figs. 1–6 and Extended Data Figs. 1–10 are provided with the paper.

Code availability

Data processing and statistical analysis algorithms from our lab can be found on our lab's Github site: https://github.com/NomuraRG, and we can make any further code from this study available at reasonable request.

References

47. Jessani, N. et al. Carcinoma and stromal enzyme activity profiles associated with breast tumor growth in vivo. *Proc. Natl Acad. Sci. USA* **101**, 13756–13761 (2004).
48. Nomura, D. K. et al. Monoacylglycerol lipase regulates a fatty acid network that promotes cancer pathogenesis. *Cell* **140**, 49–61 (2010).
49. Xu, T. et al. ProLuCID: an improved SEQUEST-like algorithm with enhanced sensitivity and specificity. *J. Proteomics* **129**, 16–24 (2015).
50. Shevchenko, A., Tomas, H., Havlis, J., Olsen, J. V. & Mann, M. In-gel digestion for mass spectrometric characterization of proteins and proteomes. *Nat. Protoc.* **1**, 2856–2860 (2006).
51. Chung, C. Y.-S. et al. Covalent targeting of the vacuolar H^+-ATPase activates autophagy via mTORC1 inhibition. *Nat. Chem. Biol.* **15**, 776–785 (2019).
52. Käll, L., Canterbury, J. D., Weston, J., Noble, W. S. & MacCoss, M. J. Semi-supervised learning for peptide identification from shotgun proteomics datasets. *Nat. Methods* **4**, 923–925 (2007).
53. Ashburner, M. et al. Gene Ontology: tool for the unification of biology. The Gene Ontology Consortium. *Nat. Genet.* **25**, 25–29 (2000).
54. The Gene Ontology Consortium. The Gene Ontology resource: 20 years and still GOing strong. *Nucleic Acids Res.* **47**, D330–D338 (2019).
55. Raudvere, U. et al. g:Profiler: a web server for functional enrichment analysis and conversions of gene lists (2019 update). *Nucleic Acids Res.* **47**, W191–W198 (2019).

Acknowledgements

We thank the members of the Nomura Research Group, Maimone Research Group and Novartis Institutes for BioMedical Research for critical reading of the manuscript.

The present study was funded by the Novartis Institutes for BioMedical Research and the Novartis-Berkeley Center for Proteomics and Chemistry Technologies. We thank F. Mapa, P. Aspesi, J. Ambrose, J. Oborski, Z. B. Kang, M. Shum and B. Cornett for their work profiling asukamycin in a panel of cancer cell lines. This work was also supported by the Nomura Research Group and the Mark Foundation for Cancer Research and Chordoma Foundation ASPIRE Award (to D.K.N. and Y.I.), and by a grant from the National Institutes of Health (grant no. R01CA240981 to D.K.N., T.J.M. and Y.I.). Y.I. and M.O. were also supported by the Japanese Society for the Promotion of Science postdoctoral fellowships.

Author contributions

Y.I., D.K.N. and T.J.M. conceived the project and wrote the paper. Y.I., J.A.T., J.M.K., L.M., M.S., S.M.B., M.D.J., X.L., W.F., T.J.M. and D.K.N. provided intellectual contributions and insights into project direction. Y.I., T.J.M., S.M.B. and D.K.N. designed the experiments. Y.I., M.O., R.W., S.M.B., X.L. and D.K.N. performed the experiments and analyzed the data. Y.I., J.A.T., J.M.K., L.M., M.S., S.M.B., M.D.J., X.L., W.F., T.J.M. and D.K.N. edited the paper.

Competing interests

J.A.T., J.M.K., L.M., M.S., S.M.B., M.D.J., X.L. and W.F. are employees of Novartis Institutes for BioMedical Research. D.K.N. is a co-founder, shareholder and adviser for Artris Therapeutics and Frontier Medicines.

Additional information

Extended data is available for this paper at https://doi.org/10.1038/s41589-020-0557-2.

Supplementary information is available for this paper at https://doi.org/10.1038/s41589-020-0557-2.

Correspondence and requests for materials should be addressed to T.J.M. or D.K.N.

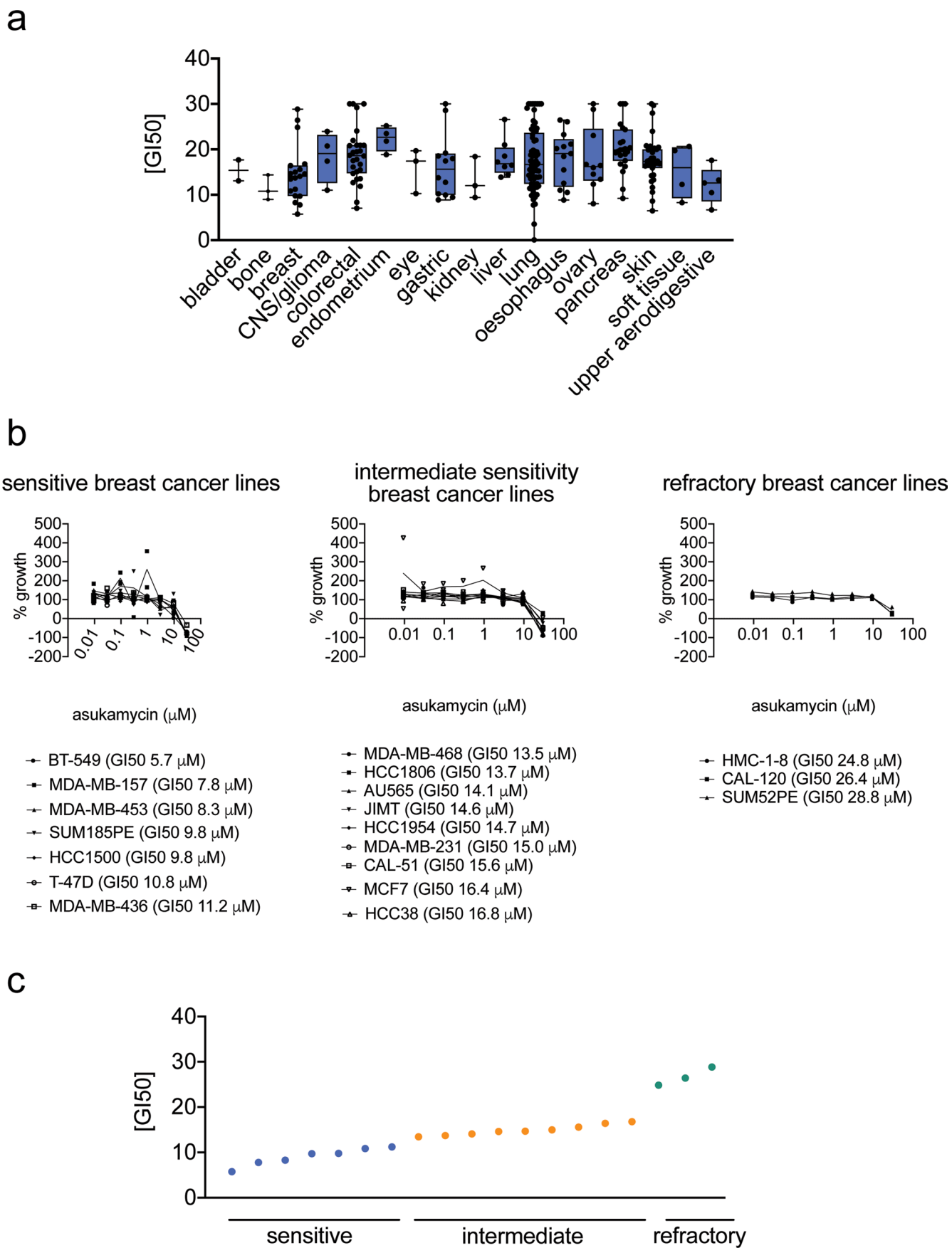

Extended Data Fig. 1 | See next page for caption.

Extended Data Fig. 1 | Testing asukamycin growth inhibitory effects across 250 cancer cell lines. a, GI50 values for asukamycin across 250 cancer cell lines by cancer tissue origin. The individual cell line data can be found in Source Data Tables for Extended Data Fig. 1. The box plot shows median, standard deviation, and minimum and maximum ranges. For bladder cancer, there were 2 cell lines; for bone cancer, 3 cell lines; breast cancer, 19 cell lines; CNS/glioma cancers, 4 cell lines; colorectal cancer, 28 cell lines; endometrial cancer, 4 cell lines; eye cancers, 3 cell lines; gastric cancers, 12 cell lines; kidney cancer, 3 cell lines; liver cancer, 8 cell lines; liver cancer, 8 cell lines; lung cancer, 73 cell lines; esophageal cancer, 13 cell lines, ovarian cancer, 10 cell lines; pancreatic cancer, 23 cell lines; skin cancer, 35 cell lines; soft tissue cancers, 4 cell lines; upper aeodigestive cancers, 5 cell lines. **b**,**c** Dose-response curves for % growth of 19 breast cancer cell lines tested **(b)** and GI50 values **(c)** for asukamycin treatment, separated by relative sensitivity to asukamycin. Data from **(a-c)** were calculated in each cell line from n = 2 biologically independent samples/group.

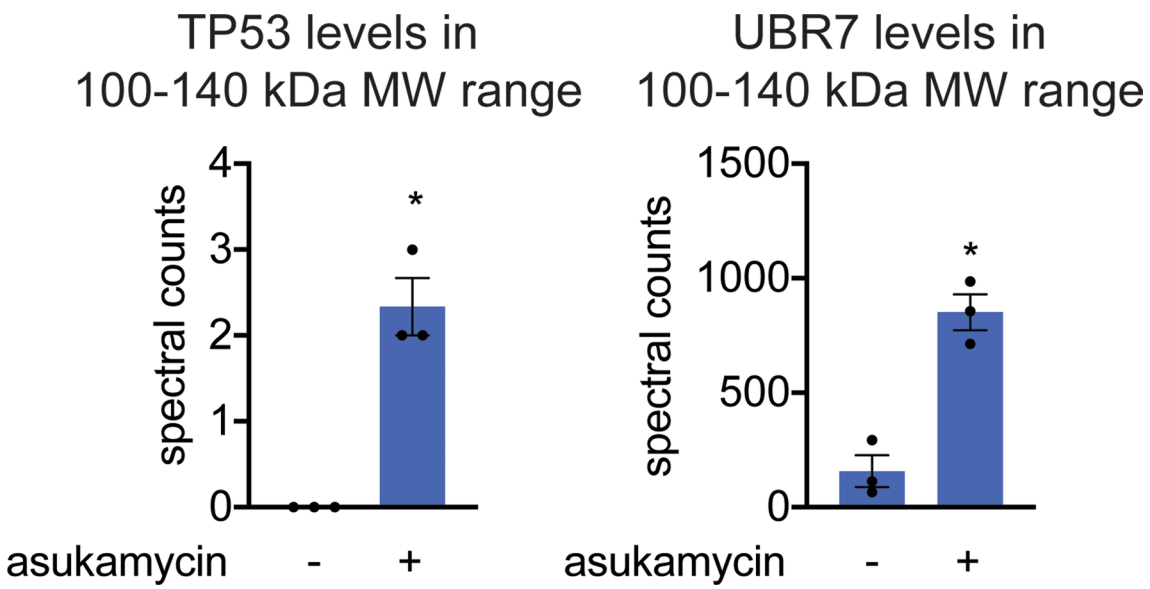

Extended Data Fig. 2 | TP53 levels in 100-140 kDa range in SDS/PAGE gel from FLAG-UBR7 pulldown. LC-MS/MS proteomic analysis of 100-140 kDa range tryptic digests of SDS/PAGE gels from FLAG-UBR7 pulldown from 231MFP cells treated with DMSO vehicle or asukamycin (50 μM) for 3 h. Data shown as individual replicate spectral count values and average ± sem and are n = 3 biologically independent samples/group. Significance was calculated by a Student's two-tailed t-test and is shown as *$p < 0.05$ in asukamycin-treated pulldown samples compared to vehicle-treated controls. Source data can be found in Source Data Tables for Extended Fig. 2.

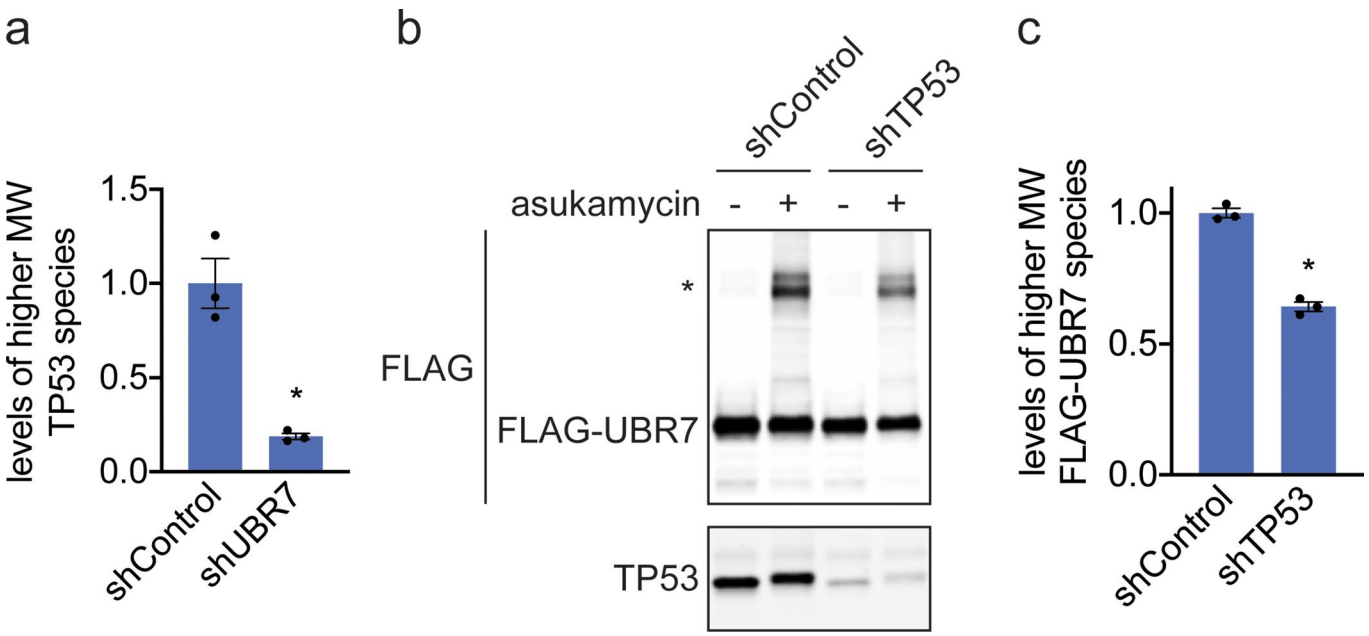

Extended Data Fig. 3 | Understanding the composition of the asukamycin-mediated higher molecular weight band. a, Quantification of TP53 levels normalized to GAPDH levels in Western blot shown in Fig. 2d. **b,** Anti-FLAG and anti-TP53 blot in shControl and shTP53 231MFP breast cancer cells expressing FLAG-UBR7 treated with vehicle DMSO or asukamycin (50 μM) for 3 h. * notes the higher molecular FLAG-UBR7 band. **c**, Quantification of higher molecular weight FLAG-UBR7 band noted with * in **(b)**. Data shown in **(a**, **c)** as individual replicate values and average ± sem and are n = 3 biologically independent samples/group. Gel shown in **(b)** is a representative gel of n = 3 biologically independent samples/group. Statistical significance was calculated with two-tailed unpaired Student's t-tests and are shown as *$p < 0.05$ compared to shControl cells treated with asukamycin in **(a, c)**. Uncropped blots can be found in Source Data for Extended Fig. 3. Source data for bar graphs can be found in Source Data Tables for Extended Fig. 3.

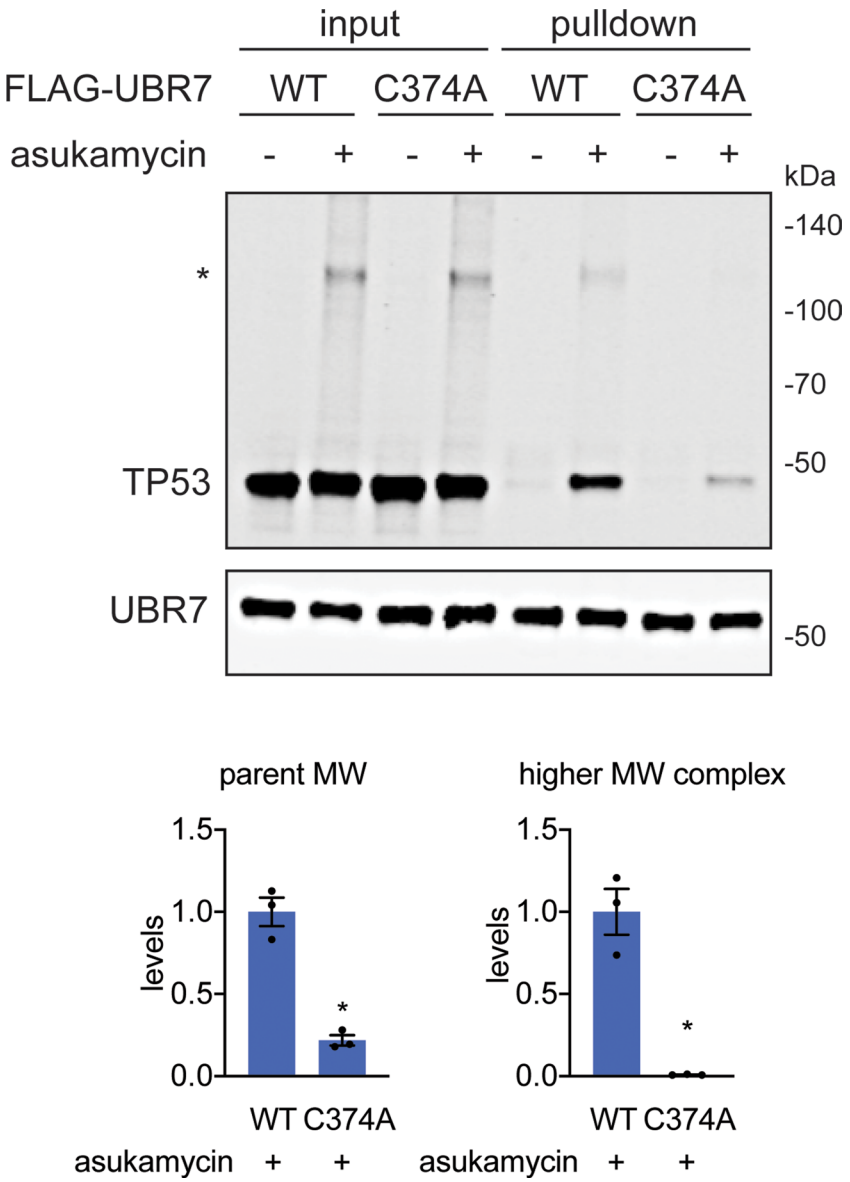

Extended Data Fig. 4 | TP53 pulldown in wild-type or C374A mutant UBR7-expressing cells. TP53 and UBR7 levels in input and pulled down eluate from FLAG-UBR7 pulldown in 231MFP cells stably expressing wild-type or C374A mutant FLAG-UBR7 in cells treated with DMSO vehicle or asukamycin (50 μM) treatment for 3 h, assessed by Western blotting. The '*' indicates the higher molecular weight (MW) TP53-asukamycin-UBR7 ternary complex. The gel is representative of n = 3 biologically independent samples/group. Bar graphs below show quantification of parent and higher molecular weight TP53 levels in asukamycin-treated FLAG-pulldown samples from wild-type and C374A-FLAG-UBR7 expressing cells. Statistical significance was calculated with two-tailed unpaired Student's t-tests and are shown as *$p < 0.05$ compared to WT asukamycin-treated groups. Uncropped blots can be found in Source Data for Extended Fig. 4. Source data for bar graphs can be found in Source Data Tables for Extended Fig. 4.

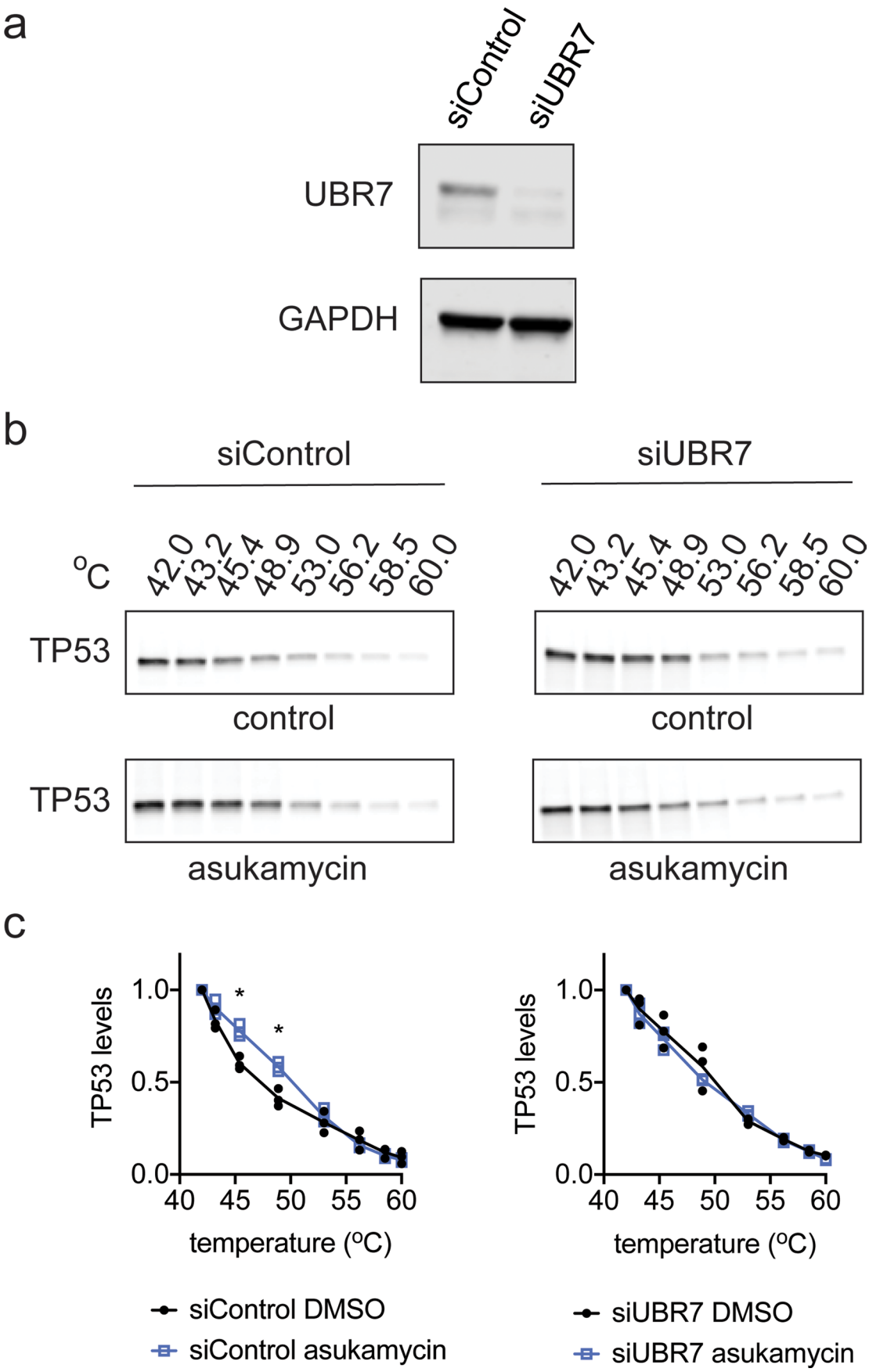

Extended Data Fig. 5 | See next page for caption.

Extended Data Fig. 5 | Thermal stability of TP53 in 231MFP cell lysate. a, UBR7 and loading control GAPDH expression in siControl and siUBR7 231MFP cells. **b**, Thermal stability of TP53 in DMSO vehicle or asukamycin (50 μM, 1 h) treated cell lysate from 231MFP siControl or siUBR7 cells. Gels are representative of n = 3 biologically independent samples/group. **c**, Quantification of thermal shift assay from **(b)**. Data in **(c)** shown as individual replicate values and average ± sem and are n = 3 biologically independent samples/group. Statistical significance in **(c)** was calculated with two-tailed unpaired Student's t-tests and are shown as $^*p < 0.05$ compared to vehicle-treated siControl groups. Data was not significant ($p > 0.05$) for all asukamycin versus DMSO comparisons in siUBR7 groups. Uncropped blots can be found in Source Data for Extended Fig. 5. Source data for plots can be found in Source Data Tables for Extended Fig. 5.

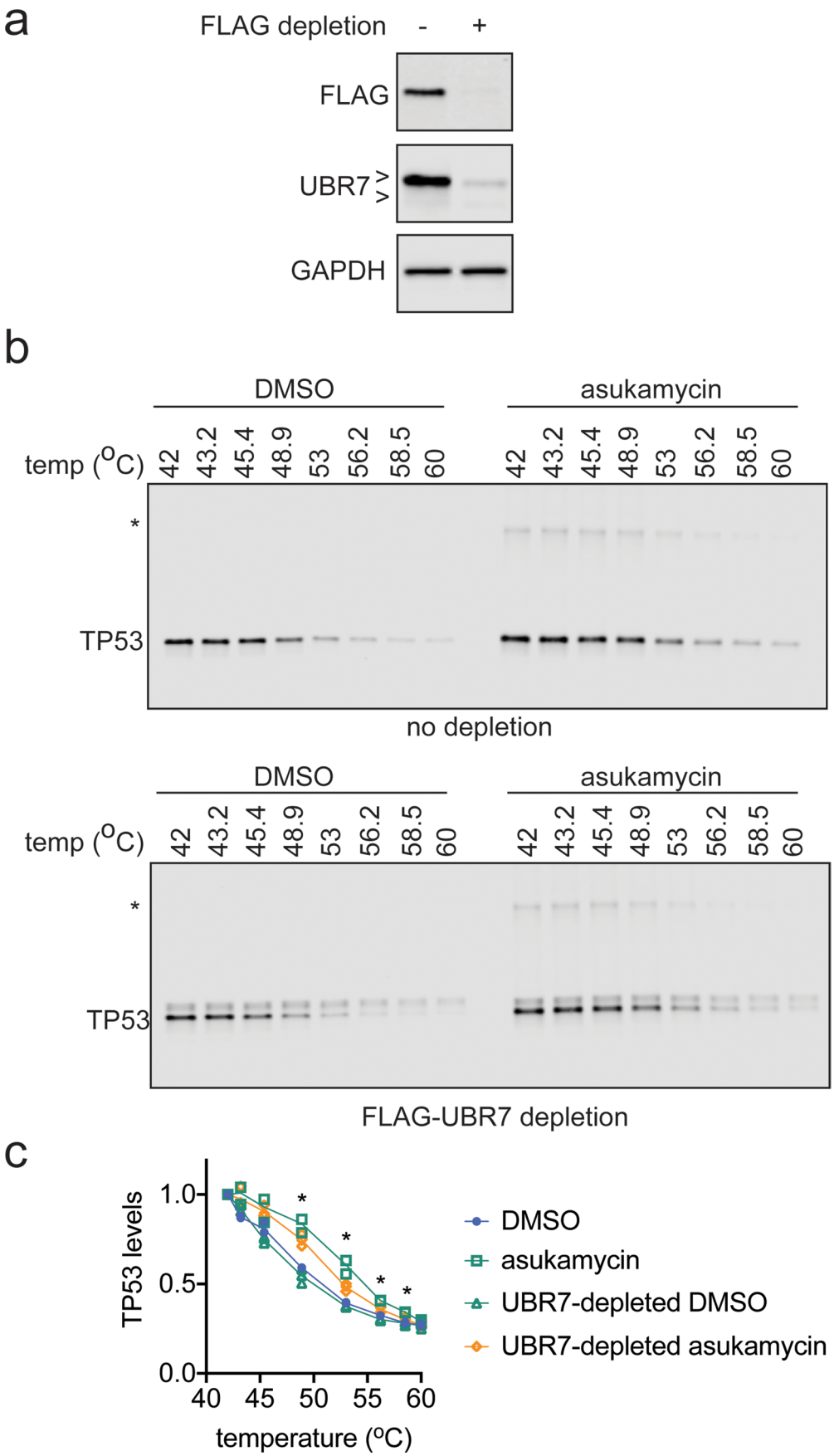

Extended Data Fig. 6 | See next page for caption.

Extended Data Fig. 6 | TP53 thermal stability. (a) FLAG-UBR7, UBR7, and loading control GAPDH levels from 231MFP cells expressing FLAG-UBR7 after mock depletion or FLAG-UBR7 depletion as assessed by Western blotting. **(b)** TP53 thermal stability in cell lysate from 231MFP FLAG-UBR7-expressing cells treated with DMSO vehicle or asukamycin (50 μM, 1h) after mock depletion or FLAG-UBR7 depletion. **(c)** Quantification of experiments described in **(b)**. Gels in **(a)** are representative of n = 3 biologically independent samples/group. Gels in **(b)** are representative of n = 3 biologically independent samples/group which are quantified and shown as individual replicate values in **(c)**. Statistical significance in **(c)** was calculated with two-tailed unpaired Student's t-tests and are shown as $*p < 0.05$ comparing UBR7-depleted asukamycin-treated groups to mock-depleted asukamycin-treated groups. Uncropped blots can be found in Source Data for Extended Fig. 6. Source data for plots can be found in Source Data Tables for Extended Fig. 6.

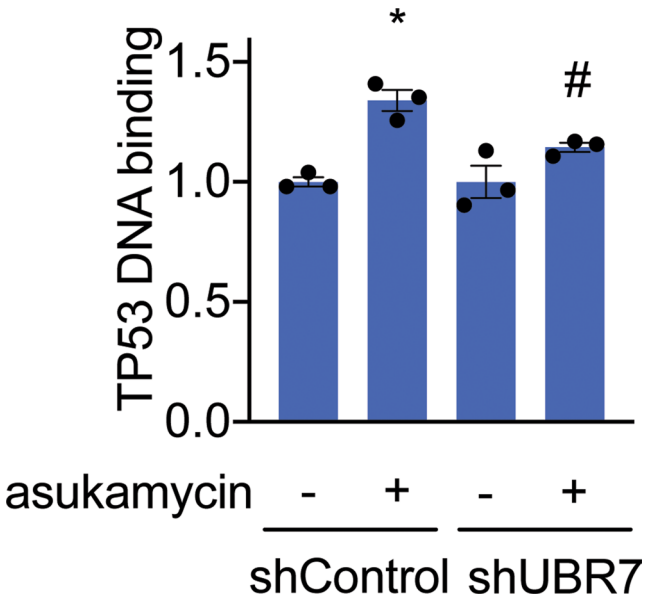

Extended Data Fig. 7 | TP53 binding to DNA consensus sequence. TP53 DNA binding to p53 DNA consensus sequence *in vitro* with TP53 spiked into 231MFP shControl or shUBR7 breast cancer cell lysate treated with DMSO vehicle or asukamycin (50 μM). Data shown are individual replicate values and average ± sem from n = 3 biologically independent samples/group. Statistical significance is calculated with two-tailed unpaired Student's t-tests and are shown as *$p < 0.05$ compared to shControl vehicle-treated groups and #$p < 0.05$ compared to shControl asukamycin-treated groups. Source data for bar graph can be found in Source Data Tables for Extended Fig. 7.

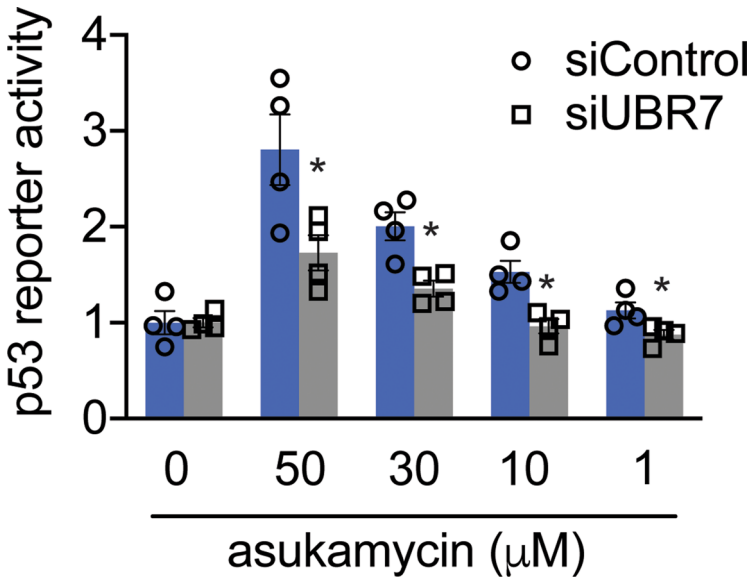

Extended Data Fig. 8 | TP53 reporter activity. TP53 reporter activity in HEK293T siControl and siUBR7 cells treated with DMSO vehicle or asukamcyin for 3 h. Data shown are individual replicate values and average ± sem from n = 4 biologically independent samples/group. Statistical significance is calculated with two-tailed unpaired Student's t-tests and are shown as *$p < 0.05$ compared to corresponding siControl treatment groups. Source data for bar graph can be found in Source Data Tables for Extended Fig. 8.

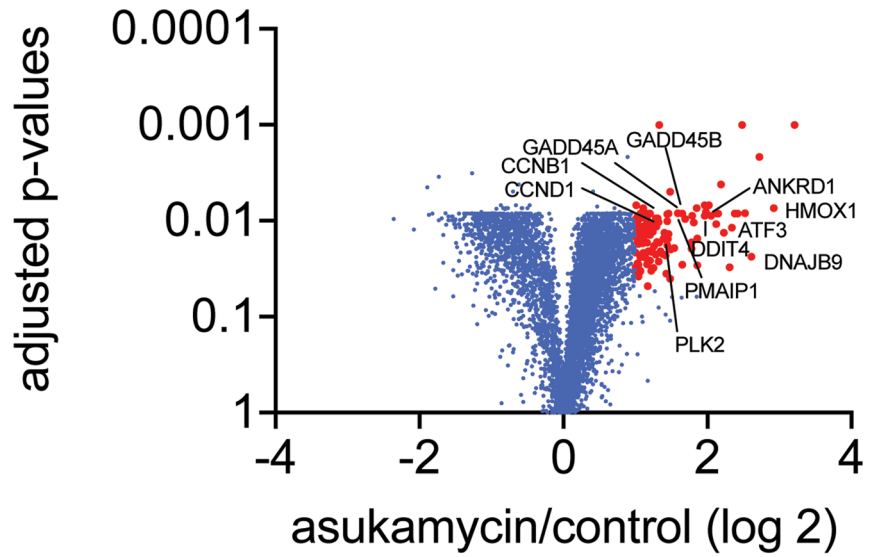

KEGG	Term ID	adjusted p-value
protein processing in the endoplasmic reticulum	KEGG:04141	1.871×10^{-7}
cellular senescence	KEGG:04218	6.874×10^{-3}
colorectal cancer	KEGG:05210	9.720×10^{-3}
MAPK signaling pathway	KEGG:04010	2.473×10^{-2}
thyroid cancer	KEGG:05216	2.636×10^{-2}
TP53 signaling pathway	KEGG:04115	3.764×10^{-2}

Extended Data Fig. 9 | Quantitative proteomic analysis of asukamycin treatment in 231MFP cells. 231MFP cells were treated with DMSO vehicle or asukamycin (50 mM, 12 h), and protein expression changes were assessed by quantitative TMT-based proteomics. Data shown are from n = 3 biologically independent samples/group. Highlighted in red are proteins in which their expression was heightened by >2-fold with adjusted p-value<0.05. The full dataset can be found in Source Data Tables for Extended Data Fig. 9. Highlighted are representative known p53 transcriptional targets. The lower table shows pathways that were significantly enriched in a functional enrichment analysis of the proteins that were upregulated by >2-fold with adjusted p-value<0.05, which includes TP53 signaling. Differential abundance significance from TMT-based proteomic data estimated using a background-based ANOVA with Benjamini-Hochberg correction to determine adjusted p-values. Statistical analysis for Pathway Enrichment Analysis was performed using the g:SCS algorithm for computing multiple testing correction for p-values gained from GO and pathway enrichment analysis. It corresponds to an experiment-wide threshold of a = 0.05. Given a fixed input query size, g:SCS analytically approximates a threshold t corresponding to the 5% upper quantile of randomly generated queries of that size. All actual p-values resulting from the query are transformed to corrected p-values by multiplying these to the ratio of the approximate threshold t and the initial experiment-wide threshold a = 0.05.

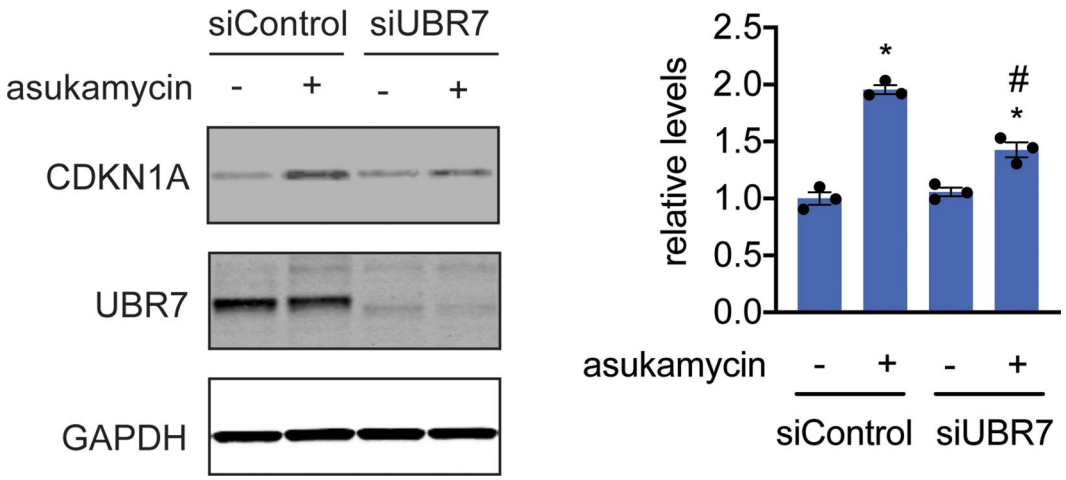

Extended Data Fig. 10 | CDKN1A level changes with asukamycin treatment. Tumor suppressor CDKN1A (p21), UBR7, and loading control GAPDH levels in 231MFP siControl and siUBR7 cells treated with DMSO vehicle or asukamycin (50 μM, 12 h), assessed by Western blotting, and quantified by densitometry and normalized to GAPDH levels. Gel on the left is representative of n = 3 biologically independent samples/group. Bar graph on the right shows individual replicate values and average ± sem from n = 3 biologically independent samples/group. Statistical significance is calculated with two-tailed unpaired Student's t-tests and are shown as *$p < 0.05$ compared to shControl vehicle-treated groups and #$p < 0.05$ compared to shControl asukamycin-treated groups. Uncropped blots can be found in Source Data for Extended Fig. 10. Source data for plots can be found in Source Data Tables for Extended Fig. 10.

nature research

Corresponding author(s): Daniel Nomura, Thomas Maimone

Last updated by author(s): 2020 04-11

Reporting Summary

Nature Research wishes to improve the reproducibility of the work that we publish. This form provides structure for consistency and transparency in reporting. For further information on Nature Research policies, see Authors & Referees and the Editorial Policy Checklist.

Statistics

For all statistical analyses, confirm that the following items are present in the figure legend, table legend, main text, or Methods section.

n/a	Confirmed	
☐	☒	The exact sample size (*n*) for each experimental group/condition, given as a discrete number and unit of measurement
☐	☒	A statement on whether measurements were taken from distinct samples or whether the same sample was measured repeatedly
☐	☒	The statistical test(s) used AND whether they are one- or two-sided *Only common tests should be described solely by name; describe more complex techniques in the Methods section.*
☒	☐	A description of all covariates tested
☐	☒	A description of any assumptions or corrections, such as tests of normality and adjustment for multiple comparisons
☐	☒	A full description of the statistical parameters including central tendency (e.g. means) or other basic estimates (e.g. regression coefficient) AND variation (e.g. standard deviation) or associated estimates of uncertainty (e.g. confidence intervals)
☐	☒	For null hypothesis testing, the test statistic (e.g. *F*, *t*, *r*) with confidence intervals, effect sizes, degrees of freedom and *P* value noted *Give P values as exact values whenever suitable.*
☒	☐	For Bayesian analysis, information on the choice of priors and Markov chain Monte Carlo settings
☒	☐	For hierarchical and complex designs, identification of the appropriate level for tests and full reporting of outcomes
☒	☐	Estimates of effect sizes (e.g. Cohen's *d*, Pearson's *r*), indicating how they were calculated

Our web collection on statistics for biologists contains articles on many of the points above.

Software and code

Policy information about availability of computer code

Data collection	Thermo XCalibur 4.0.27.10 was used to collect proteomics data
Data analysis	isoTOP-ABPP proteomics data was analyzed using Integrated Proteomics Pipeline ver 5.0.1. Statistical analysis for isoTOP-ABPP data was performed using algorithms developed in the Nomura lab and are available at https://github.com/NomuraRG. Two tailed t-tests p-values were derived using GraphPad Prism 8.4.1. TMT proteomics analysis was performed using Proteome Discoverer v. 2.2.0.388 software (Thermo) utilizing Mascot v 2.5.1 search engine. Data validation of peptide and protein identifications was done at the level of the complete dataset consisting of combined Mascot search results for all individual samples per experiment via the Percolator validation node in Proteome Discoverer. Statistical analysis for TMT proteomics data was performed in Proteome Discoverer. Functional gene enrichment statistical analysis was performed on gProfiler.

For manuscripts utilizing custom algorithms or software that are central to the research but not yet described in published literature, software must be made available to editors/reviewers. We strongly encourage code deposition in a community repository (e.g. GitHub). See the Nature Research guidelines for submitting code & software for further information.

Data

Policy information about availability of data

All manuscripts must include a data availability statement. This statement should provide the following information, where applicable:

- Accession codes, unique identifiers, or web links for publicly available datasets
- A list of figures that have associated raw data
- A description of any restrictions on data availability

All of the source data for all figures are provided. Any other additional datasets from this study are available from the corresponding authors on reasonable request.

Field-specific reporting

Please select the one below that is the best fit for your research. If you are not sure, read the appropriate sections before making your selection.

☒ Life sciences ☐ Behavioural & social sciences ☐ Ecological, evolutionary & environmental sciences

For a reference copy of the document with all sections, see nature.com/documents/nr-reporting-summary-flat.pdf

Life sciences study design

All studies must disclose on these points even when the disclosure is negative.

Sample size	No statistical test was performed to calculate sample size. The sample sizes in the study were chosen based on prior knowledge on the intrinsic variability of the experiments performed.
Data exclusions	No data were excluded from the experiments reported here.
Replication	All studies were either performed more than once and the data were reproducible, or were performed once (with appropriate biological replicates), but the results from the experiment were subsequently validated with follow-up biochemical/cell biology experiments.
Randomization	The cells used in the study were not randomized as this was not practical for experimental design.
Blinding	Investigators were not blinded to the study. Experimental data are precise measurements of protein levels and are not subjective measurements. Blinding was also not possible because each of the experiments were performed by individual researchers.

Reporting for specific materials, systems and methods

We require information from authors about some types of materials, experimental systems and methods used in many studies. Here, indicate whether each material, system or method listed is relevant to your study. If you are not sure if a list item applies to your research, read the appropriate section before selecting a response.

Materials & experimental systems

n/a	Involved in the study
☐	☒ Antibodies
☐	☒ Eukaryotic cell lines
☒	☐ Palaeontology
☒	☐ Animals and other organisms
☒	☐ Human research participants
☒	☐ Clinical data

Methods

n/a	Involved in the study
☒	☐ ChIP-seq
☒	☐ Flow cytometry
☒	☐ MRI-based neuroimaging

Antibodies

Antibodies used	Antibodies to UBR7 (PA5-31559) and p53 (DO-1) were obtained from Thermo Fisher Scientific. Antibodies to GAPDH (D16H11), Ubiquitin (P4D1), FLAG (D6W5B), p21 (12D1), Histone H2A II (2578S), p-Histone H2A.X (2577S), RPA32 (4E4), and p-RPA32/RPA2 (83745S) were obtained from Cell Signaling Technology. For all primary antibodies, a dilution of 1:1000 was used for detection. Stock and lot number information is unavailable. For dual color Western blotting, anti-mouse IR680 and anti-rabbit IR800 were used to detect TP53 (DO-1) and FLAG (D6W5B), respectively.
Validation	For UBR7 (PA5-31559) from Thermo Fisher Scientific, the vendor shows utility of antibody against human UBR7 detection in immunohistochemistry in tissues, and immunofluorescence in cells, and in Western blotting in cell lysates and shows its use in a publication. In this study, we show that UBR7 knockdown leads to a loss of the UBR7 band in cell lines and that this antibody detects overexpressed UBR7 protein in cells. For the p53 (DO-1) antibody obtained from Thermo Fisher Scientific, the vendor shows validation of antibody against human p53 in human cancer cell lysates. We show that p53 knockdown results in loss of p53 band in human cancer cells. For the GAPDH (D16H11) antibody from Cell Signaling Technologies, the vendor shows validation in Western blotting detecting human GAPDH in various human cancer cell lines. For the Ubiquitin (P4D1) antibody from Cell Signaling, the vendor shows validation in Western blotting detecting human total Ubiquitinated proteins in several human cell lines. We show that the total Ub bands present are attenuated upon treatment of human cancer cell proteome with a deubiquitinase enzyme. For the FLAG (D6W5B) antibody from Cell Signaling, the vendor shows validation of Western blotting detection for FLAG-tagged human proteins in human cell lines. We also show the expression of FLAG-UBR7 in FLAG-UBR7 expressing cells compared to

FLAG-GFP expressing control lines.

For the p21 (12D1), antibody from Cell Signaling, the vendor shows validation of Western blotting detection of human p21 in human cell lines.

For Histone H2A II (2578S), p-Histone H2A.X (2577S), RPA32 (4E4), and p-RPA32/RPA2 (83745S) obtained from Cell Signaling Technology, the vendor validates Western blotting detection for each of the human proteins in cell lines. We validate detection of these proteins in our paper using positive control chemicals known to cause DNA damage.

Eukaryotic cell lines

Policy information about cell lines

Cell line source(s)	The 231MFP cells were obtained from Prof. Benjamin Cravatt and were generated from explanted tumor xenografts of MDA-MB-231 cells purchased from ATCC as previously described in Jessani, N. et al. Carcinoma and stromal enzyme activity profiles associated with breast tumor growth in vivo. Proc. Natl. Acad. Sci. U. S. A. 101, 13756–13761 (2004). HCC38 and HEK293T cells were obtained from American Type Culture Collection (ATCC). Isogenic HCT116 colorectal cancer cell lines were generated by Novartis.
Authentication	cell lines were not authenticated
Mycoplasma contamination	mycoplasma testing was performed and found to be negative
Commonly misidentified lines (See ICLAC register)	no commonly misidentified cell lines were used.